

Calibrating Deep Neural Network using Euclidean Distance

WENHAO LIANG
Adelaide University
Adelaide, Australia
w.liang@adelaide.edu.au

CHANG GEORGE DONG
Adelaide University
Adelaide, Australia
chang.dong@adelaide.edu.au

LIANGWEI NATHAN ZHENG
Adelaide University
Adelaide, Australia
liangwei.zheng@adelaide.edu.au

ZHENGYANG DAVID LI
Adelaide University
Adelaide, Australia
zhengyang.li01@adelaide.edu.au

WEI EMMA ZHANG
Adelaide University
Adelaide, Australia
wei.e.zhang@adelaide.edu.au

WEITONG CHEN
Adelaide University
Adelaide, Australia
weitong.chen@adelaide.edu.au

ABSTRACT

Uncertainty is a fundamental aspect of real-world scenarios, where perfect information is rarely available. Humans naturally develop complex internal models to navigate incomplete data and effectively respond to unforeseen or partially observed events. In machine learning, Focal Loss is commonly used to reduce misclassification rates by emphasizing hard-to-classify samples. However, it does not guarantee well-calibrated predicted probabilities and may result in models that are overconfident or underconfident. High calibration error indicates a misalignment between predicted probabilities and actual outcomes, affecting model reliability. This research introduces a novel loss function called Focal Calibration Loss (FCL), designed to improve probability calibration while retaining the advantages of Focal Loss in handling difficult samples. By minimizing the Euclidean norm through a strictly proper loss, FCL penalizes the instance-wise calibration error and constrains bounds. We provide theoretical validation for proposed method and apply it to calibrate CheXNet for potential deployment in web-based healthcare systems. Extensive evaluations on various models and datasets demonstrate that our method achieves SOTA performance in both calibration and accuracy metrics.

CCS CONCEPTS

• **Computing methodologies** → **Machine learning**.

KEYWORDS

Probabilistic prediction, Focal Calibration Loss, Model Calibration

1 INTRODUCTION

In web-based applications, ranging from search engines to medical imaging and diagnostic systems, well-calibrated models are essential for ensuring accurate and trustworthy outcomes. Deploying such models improves the reliability of predictions and fosters user confidence in automated decision-making, whether in image classifiers [31] or large language models [1]. However, while Focal Loss, has proven effective in handling class imbalance, it often leads to overly confident predictions that are poorly calibrated [28]. A well-calibrated predictor inherently aligns its predicted probabilities with the true likelihood of events, reducing the discrepancy between the model’s confidence and actual outcomes. This alignment

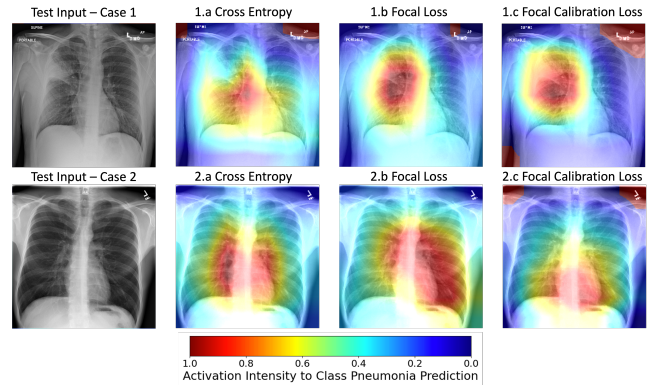


Figure 1: Grad-CAM [41] Heatmap Visualization of CheXNet Model [39] Predictions for Pneumonia Detection. This figure shows Grad-CAM heatmaps from the CheXNet model applied to two ChestX-ray14 test cases for pneumonia detection. The model predicts the probability of each thoracic disease and generates a corresponding pathology likelihood map. Subfigures (1.a, 2.a) show outputs from the model trained with cross-entropy loss; (1.b, 2.b) with focal loss; and (1.c, 2.c) with focal calibration loss, illustrating the impact of different loss functions on localizing disease-relevant regions.

minimizes the need for post-processing calibration methods, such as temperature scaling [12] or isotonic regression [37], which are typically employed to adjust miscalibrated outputs after model training. The post-processing gap is the difference between a model’s raw predictions and the calibrated probabilities required for reliable decision-making. Therefore, achieving a well-calibrated predictor directly within the loss function reduces this post-processing gap, leading to more accurate and trustworthy predictions without additional adjustments.

Motivation and Contributions Recent studies have further established the theoretical foundation of focal loss in the context of classification calibration [9]. It has been demonstrated that focal loss is classification-calibrated, implying that a classifier trained with focal loss has the potential to reach the optimal Bayes classifier. Nonetheless, training with focal loss can yield classifiers that exhibit either underconfidence or overconfidence, making it an unreliable class-posterior probability estimator. Focal loss is not a proper scoring rule, which means it does not provide an unbiased

estimation of class-posterior probabilities [9]. A proper scoring rule is designed to encourage the model to output probability estimates that match the true posterior distribution. Proper loss functions have been identified a local optimality condition necessary and sufficient for ensuring calibration [3]. Certain proper loss functions, like Log-loss and quadratic loss, achieve calibration by ensuring that the loss cannot be significantly reduced through post-processing functions with specific Lipschitz continuity guarantees. This relationship highlights the optimization of proper loss functions, such as the Brier score [5], in achieving calibration in deep learning models, as suggested by Lakshminarayanan et al. [23]. **Given the prior established benefits of proper loss functions in calibration, this research investigates whether integrating a proper loss into the focal loss can boost its calibration as a class-posterior probability estimator.** Our key contributions are as follows:

- We propose the Focal Calibration Loss (FCL), a theoretically grounded loss function that merges the traditional Focal Loss with a calibration loss term (proper loss), ensuring better probability calibration by uniquely aligning predicted probabilities with true class-posterior probabilities, thus effectively mitigating overconfidence and underconfidence.
- Through rigorous theoretical proofs, we demonstrate that minimizing the FCL yields classifiers with superior probability and classification calibration, resulting in a lower post-processing gap than with the Focal Loss alone.
- We empirically demonstrate that FCL significantly enhances model calibration and classification performance through extensive experiments on both in-distribution and out-of-distribution image and NLP datasets. Additionally, by employing the smooth calibration error (smCE) metric, we achieve more consistent calibration assessments, effectively addressing the discontinuity issues inherent in traditional bin-based metrics. FCL improves anomaly localization, recognition, and robustness in Chest X-ray imaging applications.

2 PRELIMINARIES

2.1 Problem Formulation

In multiclass classification, let \mathcal{X} denote the input space and $\mathcal{Y} = \{1, 2, \dots, K\}$ the label space, where K represents the number of classes.¹ Consider a dataset $\mathcal{D} = \{(\mathbf{x}_i, y_i)\}_{i=1}^n$ consisting of n labeled instances independently drawn from an unknown probability distribution over $\mathcal{X} \times \mathcal{Y}$ with density $p(\mathbf{x}, y)$. The goal is to find a classifier $f : \mathcal{X} \rightarrow \mathcal{Y}$ that minimizes the *classification risk* [9]:

$$\mathcal{R}^\ell(f) = \mathbb{E}_{(\mathbf{x}, y) \sim p(\mathbf{x}, y)} [\ell(f(\mathbf{x}), y)], \quad (1)$$

where $\ell(f(\mathbf{x}), y) = \mathbf{1}_{[f(\mathbf{x}) \neq y]}$ is the zero-one loss, and $\ell \in [0, 1]$. The true class-posterior probability vector is defined as $\boldsymbol{\eta}(\mathbf{x}) = [\eta_1(\mathbf{x}), \dots, \eta_K(\mathbf{x})]^\top$, where $\eta_k(\mathbf{x}) = \mathbb{P}(y = k \mid \mathbf{x})$ is the true probability of class k given input \mathbf{x} .

The Bayes-optimal classifier $f^{\ell, *}$, which minimizes the expected classification risk in Equation (1), is given by:

¹Vectors are denoted by boldface letters (e.g., \mathbf{x}), scalars by regular letters (e.g., x), and the i -th element of a vector \mathbf{x} by x_i . The indicator function is $\mathbf{1}_{[\cdot]}$, and \mathbf{x}^\top denotes the transpose of \mathbf{x} .

DEFINITION 1 (BAYES-OPTIMAL CLASSIFIER [54]). *The Bayes-optimal solution for multiclass classification is defined as:*

$$f^{\ell, *}(\mathbf{x}) = \arg \max_{y \in \mathcal{Y}} \eta_y(\mathbf{x}). \quad (2)$$

Knowing the true class-posterior probabilities $\boldsymbol{\eta}(\mathbf{x})$ allows for the determination of the Bayes-optimal classifier. However, the converse is not necessarily true [2].

2.2 Empirical Surrogate Risk

Training a neural network classifier typically involves learning a function $f : \mathcal{X} \rightarrow \Delta^K$ that maps an input $\mathbf{x} \in \mathcal{X}$ to a K -dimensional vector of predicted probabilities over the classes, denoted as $\hat{\mathbf{p}}(\mathbf{x}) = f(\mathbf{x}) = [\hat{p}_1(\mathbf{x}), \dots, \hat{p}_K(\mathbf{x})]^\top$. Here, Δ^K denotes the K -dimensional probability simplex and define the predicted probability vector as:

$$\Delta^K = \left\{ \mathbf{p} \in [0, 1]^K \mid \sum_{k=1}^K p_k = 1 \right\}. \quad (3)$$

where $\hat{p}_k(\mathbf{x})$ represents the predicted probability for class k . A common choice for f is a deep neural network with a softmax output layer. For a given input \mathbf{x} , the decision rule f^* selects the class with the highest predicted probability:

$$f^*(\mathbf{x}) = \arg \max_{y \in \mathcal{Y}} \hat{p}_y(\mathbf{x}). \quad (4)$$

Minimizing the classification risk in Equation (1) is impractical due to the finite sample size and the computational intractability of optimizing the zero-one loss because it is non-convex and non-differentiable [2, 54]. Therefore, practitioners often minimize an empirical surrogate risk instead [2, 47].

DEFINITION 2 (EMPIRICAL SURROGATE RISK [47]). *Let $\ell : \Delta^K \times \Delta^K \rightarrow \mathbb{R}$ be a surrogate loss function, and let $\mathbf{e}_{y_i} \in \{0, 1\}^K$ be the one-hot encoded vector for class y_i . The empirical surrogate risk is defined as:*

$$\hat{\mathcal{R}}^\ell(f) = \frac{1}{n} \sum_{i=1}^n \ell(f(\mathbf{x}_i), \mathbf{e}_{y_i}). \quad (5)$$

Applying regularization techniques helps mitigate overfitting [36]. The choice of an appropriate surrogate loss function is crucial, as it affects the classifier's performance. An ideal surrogate loss should be easier to optimize than the zero-one loss and ensure that minimizing the surrogate risk aligns with minimizing the expected classification risk [9].

2.3 OC and UC Definitions

DEFINITION 3 (OVERCONFIDENCE AND UNDERCONFIDENCE). *Let $f : \mathcal{X} \rightarrow \Delta^K$ be a classifier mapping inputs to predicted probabilities $\hat{\mathbf{p}}(\mathbf{x}) = f(\mathbf{x}) = [\hat{p}_1(\mathbf{x}), \dots, \hat{p}_K(\mathbf{x})]^\top$, and $\boldsymbol{\eta}(\mathbf{x}) = [\eta_1(\mathbf{x}), \dots, \eta_K(\mathbf{x})]^\top$ denote the true class-posterior probabilities. The model f is said to be: Overconfident (OC)/Underconfident (UC) at $\mathbf{x} \in \mathcal{X}$ if the highest predicted probability exceeds/less than the highest true probability:*

$$\delta_{OC}(\mathbf{x}) := \max_{k \in \mathcal{Y}} \hat{p}_k(\mathbf{x}) - \max_{k \in \mathcal{Y}} \eta_k(\mathbf{x}) > 0, \quad (6)$$

$$\delta_{UC}(\mathbf{x}) := \max_{k \in \mathcal{Y}} \hat{p}_k(\mathbf{x}) - \max_{k \in \mathcal{Y}} \eta_k(\mathbf{x}) < 0. \quad (7)$$

In other words, overconfidence occurs when the model assigns a higher probability to its most confident prediction than the true

likelihood, potentially leading to overly assertive but incorrect decisions. Underconfidence occurs when the model is less certain than warranted, which may cause hesitation in decision-making.

2.4 Calibration Error

The **Expected Calibration Error (ECE)** is a widely used metric for assessing a model’s calibration. It quantifies the difference between predicted confidences and actual accuracies. Other metrics like **Maximum Calibration Error (MCE)**, **Adaptive-ECE (AdaECE)**, and **Classwise-ECE** provide additional insights. These metrics rely on binning strategies and are formally defined in Equations (18)–(22) (Appendix A.1). However, binning methods can suffer from issues like bin size selection and data sparsity within bins. To address these limitations, the **Smooth Calibration Error (smCE)** has been proposed, which avoids discrete binning by using continuous kernel density estimation [4].

DEFINITION 4 (SMOOTH CALIBRATION ERROR [3]). Let \mathcal{H} be the family of all 1-Lipschitz functions $\eta : [0, 1] \rightarrow [-1, 1]$. For predicted probabilities $\hat{\mathbf{p}}(\mathbf{x}) = f(\mathbf{x}) = (\hat{p}_1(\mathbf{x}), \hat{p}_2(\mathbf{x}), \dots, \hat{p}_K(\mathbf{x}))$ and one-hot encoded true labels $\mathbf{y} = (y_1, y_2, \dots, y_K)$, smooth calibration error is:

$$\text{smCE}(f) := \sup_{\eta \in \mathcal{H}} \mathbb{E}_{(\mathbf{x}, \mathbf{y}) \sim \mathcal{D}} \left[\sum_{k=1}^K (y_k - \hat{p}_k(\mathbf{x})) \eta(\hat{p}_k(\mathbf{x})) \right]. \quad (8)$$

2.5 Calibration and Entropy

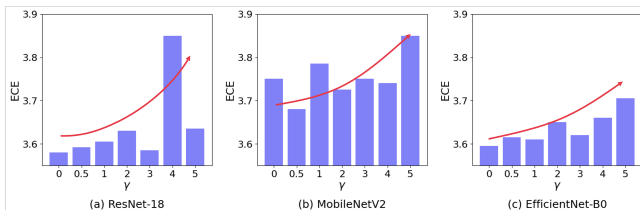


Figure 2: Impact of the focusing parameter γ on Expected Calibration Error (ECE) for (a) ResNet-18, (b) MobileNetV2, and (c) EfficientNet-B0, all trained with focal loss on CIFAR-10. Increasing γ leads to higher ECE, indicating poorer calibration.

Focal loss can be expressed in terms of the Kullback-Leibler (KL) divergence with entropy adjustments [32], as the inequality:

$$\mathcal{L}_{\text{focal}}(f(\mathbf{x}), \mathbf{y}) \geq \text{KL}(\boldsymbol{\eta}(\mathbf{x}) \| f(\mathbf{x})) + \mathbb{H}[\boldsymbol{\eta}(\mathbf{x})] - \gamma \mathbb{H}[f(\mathbf{x})], \quad (9)$$

where $\text{KL}(\boldsymbol{\eta}(\mathbf{x}) \| f(\mathbf{x}))$ is the KL divergence from the true distribution $\boldsymbol{\eta}(\mathbf{x})$ to the predicted distribution $f(\mathbf{x})$, and $\mathbb{H}[\cdot]$ denotes the entropy function (see Appendix A.9).

Calibration ensures that predicted probabilities reflect true outcome likelihoods. A well-calibrated model’s predicted probability $\hat{p}_k(\mathbf{x})$ matches the actual frequency of the outcome for class k . Focal loss adjusts the importance of examples using the focusing parameter γ . In Equation (9), the term $\text{KL}(\boldsymbol{\eta}(\mathbf{x}) \| f(\mathbf{x}))$ encourages $f(\mathbf{x})$ to approximate $\boldsymbol{\eta}(\mathbf{x})$, promoting calibration. The term $\mathbb{H}[\boldsymbol{\eta}(\mathbf{x})]$ is constant and does not affect optimization.

For low γ , focal loss favors high-entropy (less confident) predictions, aiding calibration by avoiding overconfidence. However, as γ

increases, focal loss penalizes high-entropy predictions more, potentially leading to overconfident predictions that misrepresent true likelihoods, resulting in poor calibration, as illustrated in Figure 2.

2.6 Post-Processing Gap

We define the post-processing gap as the difference between the expected calibration loss $\mathbb{E}_{(\mathbf{x}, \mathbf{y}) \sim \mathcal{D}} [\mathcal{L}_{\text{calib}}(f(\mathbf{x}), \mathbf{y})]$ and the minimal expected calibration loss achievable through post-processing $f(\mathbf{x}) \mapsto \kappa(f(\mathbf{x}))$ for some 1-Lipschitz function κ .

DEFINITION 5 (POST-PROCESSING GAP [3]). Let \mathcal{K} be the family of all post-processing functions $\kappa : [0, 1] \rightarrow [0, 1]$ such that the function $\delta(v) = \kappa(v) - v$ is 1-Lipschitz continuous. For a predictor $f : \mathcal{X} \rightarrow [0, 1]^K$ and a distribution \mathcal{D} over $\mathcal{X} \times \mathcal{Y}$, the post-processing gap $p\text{Gap}_{\mathcal{D}}(f)$ is defined as:

$$p\text{Gap}_{\mathcal{D}}(f) = \mathbb{E}_{(\mathbf{x}, \mathbf{y}) \sim \mathcal{D}} [\mathcal{L}(f(\mathbf{x}), \mathbf{y})] - \inf_{\kappa \in \mathcal{K}} \mathbb{E}_{(\mathbf{x}, \mathbf{y}) \sim \mathcal{D}} [\mathcal{L}(\kappa(f(\mathbf{x})), \mathbf{y})]. \quad (10)$$

This gap quantifies the maximum improvement in calibration achievable through optimal post-processing. It serves as a benchmark to assess how close a model’s calibration is to the best possible calibration achievable via smooth transformations.

3 PROPOSED METHOD

3.1 Focal Calibration Loss

Our observations in Figure 3 indicate that focal loss tends to produce higher-entropy predictions, resulting in outputs closer to uniform probabilities (e.g., 0.5 in binary classification). This occurs even when the true probability $\eta_k(\mathbf{x})$ is near 0 or 1 (i.e., for easy samples), leading to underconfident predictions and reduced calibration reliability. Charoenphakdee et al. [9] also demonstrated that focal loss is classification-calibrated but not strictly proper. To address calibration issues, we propose the *Focal Calibration Loss (FCL)* by adding a proper loss term to the focal loss.

Let $f : \mathcal{X} \rightarrow \Delta^K$ be a classifier mapping inputs $\mathbf{x}_i \in \mathcal{X}$ to predicted probabilities $\hat{\mathbf{p}}_i = f(\mathbf{x}_i) = [\hat{p}_{i1}, \hat{p}_{i2}, \dots, \hat{p}_{iK}]^T \in \Delta^K$. Let $\mathbf{y}_i = [y_{i1}, y_{i2}, \dots, y_{iK}]^T \in \Delta^K$ be the one-hot encoded true labels. We define the Focal Calibration Loss $\mathcal{L}_{\text{FCL}}^{\gamma, \lambda}$ as:

$$\mathcal{L}_{\text{FCL}}^{\gamma, \lambda} = \frac{1}{N} \sum_{i=1}^N [\mathcal{L}_{\text{focal}}(f(\mathbf{x}_i), \mathbf{y}_i) + \lambda \mathcal{L}_{\text{calib}}(f(\mathbf{x}_i), \mathbf{y}_i)], \quad (11)$$

where $\gamma \geq 0$ and $\lambda \geq 0$ are hyperparameters controlling the focus and calibration trade-off, respectively.

$$\mathcal{L}_{\text{focal}}(f(\mathbf{x}_i), \mathbf{y}_i) = - \sum_{k=1}^K y_{ik} (1 - \hat{p}_{ik}(\mathbf{x}_i))^\gamma \log \hat{p}_{ik}(\mathbf{x}_i), \quad (12)$$

$$\mathcal{L}_{\text{calib}}(f(\mathbf{x}_i), \mathbf{y}_i) = \|f(\mathbf{x}_i) - \mathbf{y}_i\|_2^2 = \sum_{k=1}^K (\hat{p}_{ik}(\mathbf{x}_i) - y_{ik})^2. \quad (13)$$

By directly optimizing calibration, we minimize the calibration error by reducing the Euclidean norm between $\hat{\mathbf{p}}_i$ and \mathbf{y}_i , even without access to the true class-posterior probabilities ($\boldsymbol{\eta}$). Consequently, FCL simultaneously constrains the bounds on overconfidence and underconfidence (Thm. 6) while ensuring classification calibrated with the strict propriety (Thm. 12), and achieves a smaller or equal

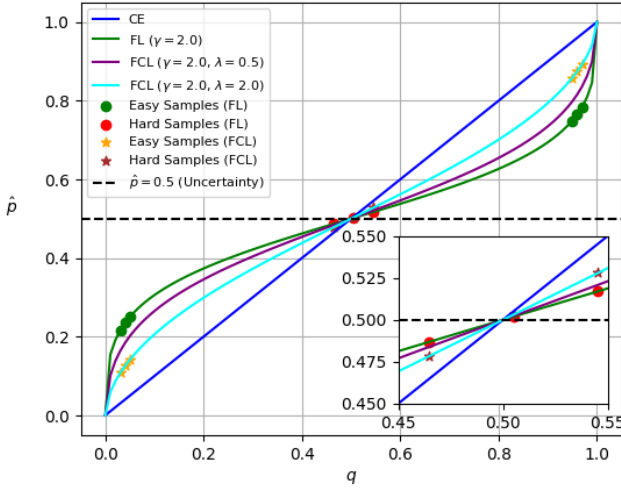


Figure 3: Binary classification ($K = 2$): Optimal predicted probabilities \hat{p} for ground-truth probabilities $q \in [0, 1]$ using Cross-Entropy Loss, Focal Loss, and Focal Calibration Loss.

post-processing gap compared to traditional focal loss (Thm. 13), thereby leading to better-calibrated models.

4 THEORETICAL EVIDENCE

4.1 Mitigate OC/UC Beyond Focal Loss

Our goal is to show that minimizing the FCL leads to predicted probabilities $\hat{p}(x)$ that are closer to $\eta(x)$, thus mitigating OC/UC.

THEOREM 6. *Let f be a classifier trained by minimizing the Focal Calibration Loss $\mathcal{L}_{\text{FCL}}^{\gamma, \lambda}$ with $\lambda > 0$. Then, for any $x \in \mathcal{X}$, the overconfidence and underconfidence are bounded by the Euclidean distance between the predicted probabilities and the true class-posterior probabilities:*

$$\left| \max_k \hat{p}_k(x) - \max_k \eta_k(x) \right| \leq \|\hat{p}(x) - \eta(x)\|_2. \quad (14)$$

Therefore, minimizing $\mathcal{L}_{\text{FCL}}^{\gamma, \lambda}$ reduces overconfidence and underconfidence by directly minimizing $\|\hat{p}(x) - \eta(x)\|_2^2$. Since the Euclidean norm aggregates the squared differences across all classes, it provides an upper bound on any individual difference (Appendix A.2 and A.3).

4.2 Classification-Calibrated

In this section, we theoretically prove that minimizing the focal calibration risk $\mathcal{R}_{\text{FCL}}^{\gamma, \lambda}$ yields the Bayes-optimal classifier, which ensures the highest possible expected accuracy in classification tasks [54]. To demonstrate this, we show that the Focal Calibration Loss (FCL) is classification-calibrated [2, 45].

DEFINITION 7. (Pointwise Conditional Risk). *The pointwise conditional risk $\mathcal{R}^{\mathcal{L}}$ of an input x with its class-posterior probability $\eta(x)$*

is defined as:

$$\mathcal{R}^{\mathcal{L}}(q(x); \eta(x)) = \sum_{y \in \mathcal{Y}} \eta_y(x) \mathcal{L}(q(x), e_y). \quad (15)$$

Intuitively, the pointwise conditional risk $\mathcal{R}^{\mathcal{L}}$ corresponds to the expected penalty for a data point x when using $q(x)$ as a score function. $\mathcal{L}(q(x), e_y)$ denotes the loss incurred by predicting $q(x)$ when the true class is y , where $e_y \in \{0, 1\}^K$ is a one-hot encoded vector corresponding to class y .

DEFINITION 8. (Classification-Calibrated Loss [2, 45]). *Consider a surrogate loss \mathcal{L} . Let $q^{\mathcal{L},*} = \arg \min_q \mathcal{R}^{\mathcal{L}}(q(x); \eta(x))$ be the minimizer of the pointwise conditional risk. \mathcal{L} is classification-calibrated, if $\mathcal{R}^{\mathcal{L}_{0-1}}(f q^{\mathcal{L},*}) = \mathcal{R}^{\mathcal{L}_{0-1}}(f \mathcal{L}_{0-1,*})$.*

Classification calibration guarantees that the minimizer of the pointwise conditional risk of a surrogate loss will yield the Bayes-optimal classifier. This definition suggests that by minimizing a classification-calibrated loss, even if $q^{\mathcal{L},*}(x)$ is not equal to the true class-posterior probability $\eta(x)$, we can still achieve the Bayes-optimal classifier from $q^{\mathcal{L},*}(x)$ as long as their decision rules match.

DEFINITION 9. (Strictly Order-Preserving Property). *Let \mathcal{X} be the input space, and $\mathcal{Y} = \{1, 2, \dots, K\}$ be the label space with K classes. For an input sample $x \in \mathcal{X}$, let $q = [q_1(x), q_2(x), \dots, q_K(x)]^\top$ denote the predicted probability distribution over the K classes, and $\eta(x) = [\eta_1(x), \eta_2(x), \dots, \eta_K(x)]^\top$ denote the true class-posterior probability distribution. Let $\mathcal{L}(q, y)$ be a loss function, where q is the predicted probability distribution and y is the true label. Formally, let $q_i^{\mathcal{L},*}(x)$ denote the minimizer of the pointwise conditional risk $\mathcal{R}^{\mathcal{L}}(x)$. The loss function \mathcal{L} is classification-calibrated if and only if:*

$$q_i^{\mathcal{L},*}(x) < q_j^{\mathcal{L},*}(x) \Rightarrow \eta_i(x) < \eta_j(x). \quad (16)$$

for all $i, j \in \{1, 2, \dots, K\}$ and for all $x \in \mathcal{X}$. This ensures that the predicted probabilities' order matches the true probabilities' order, leading to a Bayes-optimal classifier.

A loss function is said to be *classification-calibrated* if it satisfies the strictly order-preserving property. This property ensures that the minimizer of the pointwise conditional risk preserves the order of the true class-posterior probabilities. To simplify notation, we use $q^{\gamma, \lambda, *}$ to denote $q^{\mathcal{L}_{\text{FCL}}^{\gamma, \lambda}, *}$, i.e., the focal calibration risk minimizer with parameters γ and λ . Since $q^{\gamma, \lambda, *}$ preserves the order of η , it follows that $\arg \max_y q_y^{\gamma, \lambda, *}(x) = \arg \max_y \eta_y(x)$. Thus, the Bayes-optimal classifier can be achieved by minimizing the focal calibration risk minimizer, i.e., $\mathcal{R}^{\mathcal{L}_{0-1}}(f q^{\gamma, \lambda, *}) = \mathcal{R}^{\mathcal{L}_{0-1}}(f \mathcal{L}_{0-1,*})$. Our proof demonstrates that the FCL possesses the strictly order-preserving property (Appendix A.5), which is sufficient for classification calibration [54]. The following theorem guarantees that the focal calibration loss is classification-calibrated.

4.3 Strictly Proper

In this section, we examine the FCL in the context of class-posterior probability estimation. We theoretically demonstrate that the simplex output of the focal calibration risk minimizer $q^{\gamma, \lambda, *}$ does not produce the true class-posterior probability. To be suitable for class-posterior probability estimation, a surrogate loss must be strictly proper, defined as follows.

DEFINITION 10. (Strictly Proper Loss [7, 11, 42]). We say that a loss $\mathcal{L} : \Delta^K \times \Delta^K \rightarrow \mathbb{R}$ is strictly proper if $\mathcal{L}(\hat{\mathbf{p}}, \mathbf{y})$ is minimized iff $\hat{\mathbf{p}} = \mathbf{y}$.

Strict properness can be viewed as a fundamental requirement for a loss function when estimating the true class-posterior probability [49]. When comparing the ground truth probability \mathbf{y} and its estimate $\hat{\mathbf{p}}$, we want the loss function to be minimized if and only if $\hat{\mathbf{p}} = \mathbf{y}$, indicating that the probability estimation is correct. Strict properness is a more stringent requirement than classification calibration since all strictly proper losses are classification-calibrated; however, the reverse does not hold true [40, 49]. While focal loss has been proven to be not strictly proper, we demonstrate that calibration loss is strictly proper in Thm. 11 (Appendix A.7), and focal calibration loss is strictly proper in Thm. 12 (Appendix A.8).

THEOREM 11. The calibration loss defined as the mean squared L_2 norm, $\mathcal{L}_{\text{calib}}(f(\mathbf{x}_i), \mathbf{y}_i) = \|f(\mathbf{x}_i) - \mathbf{y}_i\|_2^2 = \sum_{k=1}^K (\hat{p}_{ik} - y_{ik})^2$, is a strictly proper scoring rule for both binary and multiclass classification.

THEOREM 12. The Focal Calibration Loss $\mathcal{L}_{\text{FCL}}^{\gamma, \lambda}$ is strictly proper iff $\lambda > 0$ and $\gamma \geq 0$.

4.4 Reduction of Post-Processing Gap

THEOREM 13. For any predictor $f : \mathcal{X} \rightarrow [0, 1]$ and any distribution \mathcal{D} over $\mathcal{X} \times \{0, 1\}$, the focal calibration loss $\mathcal{L}_{\text{FCL}}^{\gamma, \lambda}$ results in a smaller or equal post-processing gap compared to the focal loss:

$$p\text{Gap}_{\mathcal{D}}(\mathcal{L}_{\text{FCL}}) \leq p\text{Gap}_{\mathcal{D}}(\mathcal{L}_{\text{focal}}). \quad (17)$$

Thm. 13 indicates that incorporating the calibration loss term into the FCL objective function effectively reduces the potential improvement achievable through post-processing. This suggests that models trained with FCL are inherently better calibrated, as it reduces the calibration error (Appendix A.14).

5 EXPERIMENTAL RESULTS

We evaluate the effectiveness of our proposed method on both image and text classification tasks. For **image classification**, we utilize datasets such as CIFAR-10/100 [19], Tiny-ImageNet [10], and CheXNet [39] to evaluate calibration of models including ResNet50 [13], ResNet-100 [14], Wide-ResNet-26-10 [53], and DenseNet-121 [16]. For **text classification**, we employ the 20 Newsgroups dataset [24], web news dataset AG News [55] and FinSen [25], training with global-pooling CNN [26]. More, we include Out-of-Distribution (OoD) datasets to evaluate the robustness of the models: the SVHN dataset [35], which consists of street view house numbers, and the CIFAR-10-C dataset [15], a corrupted version of the CIFAR-10.

Baselines Among calibration-during-training methods, Cross Entropy with Weight Decay (5×10^{-4}) [12], MMCE [22], Brier loss [5], Label Smoothing (LS-0.05) [43], sample-dependent focal loss (FLSD-53) [28], and Dual Focal Loss [44] as baselines. For post hoc calibration, we report the effect of temperature scaling [12] on top of these methods. For temperature scaling, we select the optimal temperature $T \in (0, 10]$ (step size 0.1) that gives the lowest ECE on the validation set.

Experiment Setup Our experiment setup aligns with prior work and public code by Mukhoti et al. [32] implemented using PyTorch. CIFAR-10/100: Trained ResNet-50, ResNet-110, WideResNet, DenseNet for 350 epochs, with a learning rate set to 0.1 for the first 150 epochs, 0.01 for the following 100 epochs, and 0.001 for the remaining epochs. Tiny-ImageNet: Trained ResNet for 100 epochs, with a learning rate set to 0.1 for the first 40 epochs, 0.01 for the following 20 epochs, and 0.001 for the remaining epochs. 20 Newsgroups: Trained Global Pooling CNN for 50 epochs, with a learning rate set to 0.001, beta set from 0.9 to 0.999. We used Glove word embedding (glove.6B.100d) to train and evaluated by the best validated models. CheXNet: Trained DenseNet for 100 epochs with a ReduceLROnPlateau scheduler (patience = 5). For optimization, we used SGD with a weight decay of 5×10^{-4} and momentum of 0.9 for CIFAR-10/100 and Tiny-ImageNet, Adam optimizer with a learning rate of 0.001 for 20Newsgroup, and Adam optimizer with a learning rate of 0.0001 for CheXNet with 1×10^{-5} weight decay. The batch sizes are all set to 128 but 32 for CheXNet. All experiments were conducted on NVIDIA GeForce RTX 3060 Ti and NVIDIA GeForce RTX 4090, with random seeds set to 1. For temperature scaling results, the temperature parameter T was optimized through a grid search over the range $T \in [0, 0.1, 0.2, \dots, 10]$ on the validation set, based on the best post-temperature-scaling ECE. The exact temperature parameter was also used for other metrics, such as AdaECE, Classwise-ECE and smCE.

5.1 Calibration Performance

5.1.1 Calibration Error. Tables 1, 3, 6, and 7 present the ECE, smCE, AdaECE, and Classwise-ECE metrics, respectively, before (pre) and after (post) temperature scaling for different methods across various models and datasets. Overall, FCL consistently achieves lower pre-T calibration error compared to other methods, indicating better inherent calibration. Post-T calibration error for FCL are also among the lowest, showcasing its effectiveness even after temperature scaling. FCL performs well across different architectures, particularly excelling with DenseNet-121 and ResNet-50/110. It demonstrates strong performance on CIFAR-10, CIFAR-100, and Tiny-ImageNet, with significant improvements in calibration. These results underscore the efficacy of FCL in enhancing model calibration, outperforming other methods like Brier Loss, MMCE, and Label Smoothing. Focal Loss in both pre- and post-temperature scaling scenarios.

5.1.2 Reliability Diagram. The Fig. 9 for ResNet-110 trained on CIFAR-10 show the reliability diagram for different loss functions: Cross Entropy, FLSD-53, Dual Focal, and Focal Calibration. The Cross Entropy loss shows a significant gap between the expected and actual accuracy, especially in the higher confidence bins indicated poor calibration. Focal Calibration Loss achieves the best

²We follow the experimental methodology of Mukhoti et al. (2020) [32], utilizing their publicly available code [33]. For the Dual Focal Loss, we initially set $\gamma = 5$ based on preliminary tuning reported by Tao et al. (2023) [44] to ensure a fair comparison. Since specific γ values for other models and datasets were not provided, we performed cross-validation to determine the optimal γ for each experiment. These optimized γ values may influence the observed results by enhancing model calibration and performance. Optimal temperature scaling values determined by validation set (included in brackets) close to 1.0 indicate well-calibrated predictions requiring minimal adjustment.

³The smCE metrics is based on the approach presented by Blasiok and Nakkiran [4], with the corresponding implementation publicly available on GitHub [8].

Table 1: ↓ ECE (%) for various methods both before (pre) and after (post) applying temperature scaling (Bin = 15)².

Dataset	Model	Weight Decay[12]		Brier Loss[5]		MMCE[22]		Label Smooth[43]		Focal Loss - 53[32]		Dual Focal[44]		Focal Calibration	
		Pre T	Post T	Pre T	Post T	Pre T	Post T	Pre T	Post T	Pre T	Post T	Pre T	Post T	Pre T	Post T
CIFAR-100	ResNet-50	18.02	2.60(2.2)	5.47	3.71(1.1)	15.05	3.41(1.9)	6.38	5.12(1.1)	5.54	2.28(1.1)	8.79	2.31(1.3)	3.71	2.14(1.1)
	ResNet-110	19.29	4.75(2.3)	6.72	3.59(1.2)	18.84	4.52(2.3)	9.53	5.20(1.3)	11.02	3.88(1.3)	11.65	3.75(1.3)	4.19	3.23(1.1)
	Wide-ResNet-26-10	15.17	2.82(2.1)	4.07	3.03(1.1)	13.57	3.89(2.0)	3.29	3.29(1.0)	2.42	2.16(1.1)	5.30	2.27(1.2)	2.22	2.22(1.0)
	DenseNet-121	19.07	3.42(2.2)	4.28	2.22(1.1)	17.37	3.22(2.0)	8.63	4.82(1.1)	3.40	1.55(1.1)	6.69	1.65(1.2)	1.31	1.31(1.0)
CIFAR-10	ResNet-50	4.23	1.37(2.5)	1.83	0.96(1.1)	4.67	1.11(2.6)	4.23	1.87(0.9)	1.46	1.46(1.0)	1.32	1.32(1.0)	0.76	0.76(1.0)
	ResNet-110	4.86	1.94(2.6)	2.50	1.36(1.2)	5.22	1.24(2.8)	3.74	1.22(0.9)	1.67	1.10(1.1)	1.48	1.27(1.1)	0.95	0.95(1.0)
	Wide-ResNet-26-10	3.24	0.86(2.2)	1.07	1.07(1.0)	3.60	1.26(2.2)	4.66	1.27(0.8)	1.83	1.17(0.9)	3.35	0.94(0.8)	0.92	0.92(1.0)
	DenseNet-121	4.70	1.54(2.4)	1.24	1.24(1.0)	4.97	1.71(2.4)	4.05	1.01(0.9)	1.73	1.22(0.9)	0.70	1.31(0.9)	0.66	0.66(1.0)
Tiny-ImageNet	ResNet-50	16.03	5.23(1.5)	5.12	3.49(0.9)	13.15	4.77(1.3)	15.05	5.35(0.7)	1.61	1.61(1.0)	2.69	2.69(1.0)	10.22	1.35(0.8)
NLP 20 Newsgroups	Global Pooling CNN	17.92	2.39(2.3)	15.48	6.78(2.1)	15.38	3.22(1.9)	4.79	2.54(1.1)	6.92	2.19(1.1)	18.45	3.89(2.3)	15.35	1.54(2.2)
NLP AG News	Global Pooling CNN	4.82	0.67(2.0)	6.83	2.73(2.8)	1.87	1.79(1.1)	3.90	1.62(0.8)	6.70	0.87(3.0)	2.87	2.44(0.8)	0.99	0.34(1.1)
NLP FinSen	Global Pooling CNN	0.98	0.44(2.5)	0.54	0.54(1.0)	1.23	0.92(0.5)	4.41	0.53(0.6)	0.43	0.53(0.9)	0.40	0.50(0.7)	0.51	0.31(1.3)

Table 2: ↓ Classification error (%) on test set across different methods.

Dataset	Model	Weight Decay [12]	Brier Loss [5]	MMCE [22]	Label Smooth [43]	Focal Loss - 53 [32]	Dual Focal[44]	Focal Calibration
CIFAR-100	ResNet-50	22.75	25.29	22.16	23.03	22.44	21.97	21.81
	ResNet-110	22.93	24.79	22.78	22.98	22.04	21.73	21.02
	Wide-ResNet-26-10	20.64	20.45	20.59	20.36	19.89	20.05	19.81
	DenseNet-121	24.20	23.83	23.70	21.85	22.84	23.00	21.80
CIFAR-10	ResNet-50	4.87	5.17	5.14	4.72	4.94	5.70	4.56
	ResNet-110	5.20	5.34	5.56	4.70	5.19	5.82	4.75
	Wide-ResNet-26-10	3.80	4.46	4.22	4.12	4.34	4.12	4.16
	DenseNet-121	5.11	4.82	5.36	4.79	5.46	5.39	4.59
Tiny-ImageNet	ResNet-50	50.36	53.47	51.57	47.93	48.84	49.73	47.68
20 Newsgroups	Global Pooling CNN	27.66	27.16	28.41	28.03	31.16	28.93	27.13
AG News	Global Pooling CNN	8.86	8.53	8.21	8.33	8.84	8.28	8.13
FinSen	Global Pooling CNN	1.13	1.26	1.42	1.13	1.22	1.09	1.22

Table 3: ↓ smCE (%) for various methods both before (pre) and after (post) applying temperature scaling³.

Dataset	Model	Weight Decay[12]		Brier Loss[5]		MMCE[22]		Label Smooth[43]		Focal Loss - 53[32]		Dual Focal[44]		Focal Calibration	
		Pre T	Post T	Pre T	Post T	Pre T	Post T	Pre T	Post T	Pre T	Post T	Pre T	Post T	Pre T	Post T
CIFAR-100	ResNet-50	14.95	2.63(2.2)	5.34	3.53(1.1)	13.40	3.12(1.9)	6.31	3.43(1.1)	5.56	2.37(1.1)	8.82	2.24(1.3)	3.68	2.29(1.1)
	ResNet-110	15.05	3.84(2.3)	6.53	3.51(1.2)	14.86	3.51(2.3)	9.55	4.36(1.3)	10.98	3.60(1.3)	11.69	3.31(1.3)	4.16	3.08(1.1)
	Wide-ResNet-26-10	12.97	2.85(2.1)	4.06	2.78(1.1)	12.27	3.85(2.0)	3.04	3.04(1.0)	2.34	2.20(1.1)	6.01	2.41(0.9)	2.16	2.16(1.0)
	DenseNet-121	15.42	2.61(2.2)	3.86	1.93(1.1)	15.96	2.95(2.0)	3.85	3.68(1.1)	3.04	1.50(1.1)	4.07	1.72(0.9)	1.48	1.48(1.0)
CIFAR-10	ResNet-50	3.27	1.48(2.5)	1.83	1.27(1.1)	3.41	1.47(2.6)	3.31	1.92(0.9)	1.45	1.45(1.0)	1.36	1.36(1.0)	0.99	0.99(1.0)
	ResNet-110	3.43	1.88(2.6)	2.49	1.63(1.2)	3.38	1.55(2.8)	2.87	1.52(0.9)	1.69	1.39(1.1)	1.48	1.35(1.1)	1.17	1.17(1.0)
	Wide-ResNet-26-10	2.70	1.25(2.2)	1.55	1.55(1.0)	3.03	1.46(2.2)	3.75	1.47(0.8)	1.84	1.46(0.9)	3.31	1.20(0.8)	1.16	1.16(1.0)
	DenseNet-121	15.42	2.61(2.4)	3.86	1.93(1.0)	15.96	2.95(2.4)	2.84	1.63(0.9)	3.04	1.50(0.9)	4.07	1.72(0.9)	1.48	1.48(1.0)
Tiny-ImageNet	ResNet-50	15.80	5.02(1.5)	5.02	3.50(0.9)	13.02	4.65(1.3)	14.99	5.24(0.7)	1.46	1.46(1.0)	6.78	1.99(0.9)	10.23	1.39(0.8)
NLP 20 Newsgroups	Global Pooling CNN	17.33	2.41(2.7)	15.13	1.85(2.2)	13.51	2.17(2.1)	4.77	7.40(0.8)	6.20	4.19(1.1)	10.95	3.54(1.8)	14.91	1.59(2.2)
NLP AG News	Global Pooling CNN	4.56	0.80(2.0)	5.63	2.72(2.8)	1.78	1.75(1.1)	3.83	1.55(0.8)	6.07	0.75(3.0)	2.74	2.34(0.8)	1.12	0.60(1.1)
NLP FinSen	Global Pooling CNN	0.88	0.66(2.5)	0.76	0.76(1.0)	1.30	0.91(0.5)	4.44	0.65(0.6)	0.68	0.68(0.9)	0.63	0.66(0.7)	0.72	0.65(1.3)

calibration among the methods, with the lowest ECE and a relatively low MCE. The expected and actual accuracies are closely aligned, indicating excellent calibration. Additionally, it has the lowest test error, demonstrating that FCL not only improves calibration but also maintains or improves classification performance. The Fig. 10 for ResNet-50 trained on CIFAR-10 with epochs range from 100 to 300 also proves it.

5.2 Classification Performance

5.2.1 Classification Error. The Tab. 2 presents the classification error (%) on the test set for various methods across different datasets

and models. FCL consistently achieves the lowest classification error in most cases across all datasets and models, demonstrating its effectiveness in reducing test errors.

5.3 Gradient-Based Localization

5.3.1 Grad-CAM Heatmaps on CheXNet. We evaluate the effects of Cross Entropy, Focal Loss, and Focal Calibration Loss on localization performance using Grad-CAM heatmaps, a popular visualization technique for identifying regions of interest in deep learning models [41]. Fig. 1 presents a comparison of heatmaps generated with each loss function applied to CheXNet [39], a deep learning model for

chest X-ray classification. For Cross Entropy, the heatmaps show broader regions of activation, which suggest that the model has less certainty in localizing the anomalies. In contrast, focal loss demonstrates more concentrated regions of activation. This suggests that focal loss sharpens the model’s focus on challenging examples. However, while the activations are more focused, they may not always be aligned with precise boundaries, which could affect the confidence in anomaly localization. Focal Calibration Loss, on the other hand, provides the most well-defined and precise activation areas. The heatmaps generated show a balanced focus, particularly in difficult cases, while also improving probability calibration. This results in clearer boundaries and more accurate localization of anomalies lead to more confident and reliable predictions, making it especially suited for medical diagnosis tasks where precise localization and confidence in predictions are critical. Thus, FCL not only enhances model calibration but also refines anomaly localization, offering substantial benefits for applications in medical imaging where accurate and confident diagnoses are of utmost importance.

5.4 Robustness on OoD Data Shift

We assess the robustness of models trained on in-distribution CIFAR-10 and evaluated on two distinct out-of-distribution (OoD) datasets: SVHN and CIFAR-10-C. Tab. 4 presents the performance of Area Under the Receiver Operating Characteristic curve (AUROC) under data shifts. Across most datasets, FCL consistently achieves the highest AUROC, outperforming other models in handling OoD data. This indicates that FCL enhances the model’s ability to distinguish between in-distribution and out-of-distribution samples effectively. This suggests that the robustness improvements introduced by FCL generalize well across different types of OoD shifts.

5.5 Discussion

5.5.1 Faster convergence. In our experiments, we compared the performance of various loss functions on the CIFAR-10 dataset using a ResNet-110 architecture. Specifically, we evaluated CE, FL ($\gamma=3.0$), DFL ($\gamma=2.0$), and FCL ($\gamma=3.0$). The results, depicted in Figure 4, illustrate the normalized test loss across training epochs. During the initial epochs from 0 to 50, CE demonstrated a relatively stable decrease, while the FL showed higher variability with sharp peaks and troughs, indicating potential overfitting on hard examples. The FCL shows faster convergence, reaching a low normalized test loss more quickly than the other loss functions. This indicates that FCL might be more effective in stabilizing and minimizing the loss during the initial training phase. From epochs 50 to 150, all loss functions exhibited a reduction in variability, but the FCL and DFL consistently showed the lowest and most stable loss values with similar pattern after epoch 150.

5.5.2 Balance between γ and λ . We compared the FCL and FL with different λ values while keeping $\gamma = 3.0$ constant by metrics including NLL, ECE, AdaECE, and Classwise-ECE both before and after temperature scaling as well as test error for each λ in Fig. 5. NLL decreases initially as λ increases from 0 to 0.5 but shows fluctuations and a slight increase beyond $\lambda = 1.5$. For post-temperature scaling, NLL values are generally lower, indicating improved calibration. ECE decreases significantly when λ is 0.5, indicating improved calibration. However, calibration error increases for higher λ values,

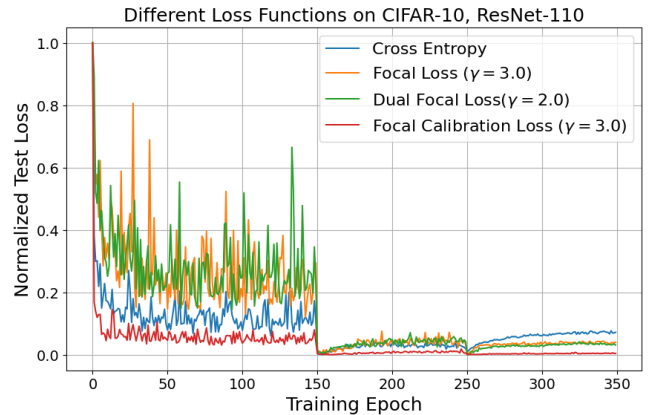


Figure 4: Normalized test loss across training epochs for different loss functions on CIFAR-10 using ResNet-110. The comparison includes Cross Entropy, Focal Loss ($\gamma=3.0$), Dual Focal Loss ($\gamma=2.0$), and Focal Calibration Loss ($\gamma=3.0$). Focal Calibration Loss with faster convergence and stability.

suggesting that too much regularization might degrade calibration performance as depicted in Fig. 5. The experiment shows that $\lambda = 0.5$ provides the best calibration performance across all ECE metrics before and after temperature scaling. Adjusting γ influences how much the model concentrates on hard examples—higher γ increases this focus, which can improve calibration but may also lead to overfitting if excessive. Modifying λ controls the weight of the calibration loss component; increasing λ emphasizes probability calibration by penalizing deviations between predicted and true probabilities, but overly large values can reduce classification accuracy. Therefore, appropriate tuning of these hyperparameters is crucial to achieving a desirable balance between calibration and classification effectiveness. We provide table of γ and λ selection with best calibration error performance in Appendix A.10.

5.5.3 Temperature scaling and post-processing gap. To empirically validate the theoretical reduction in post-processing gap as Theorem 13, we compare the ECE/smCE/AdaECE/Classwise-ECE of models trained with focal loss and FCL before and after temperature scaling. As shown in Tab. 1, Tab. 3, Tab. 6 and Tab.7, the focal loss model exhibits a significant reduction in ECE after temperature scaling, indicating a substantial post-processing gap. In contrast, the FCL model shows minimal change in ECE after temperature scaling closing with 1.0, particularly in smCE, confirming that FCL effectively reduces the post-processing gap during training.

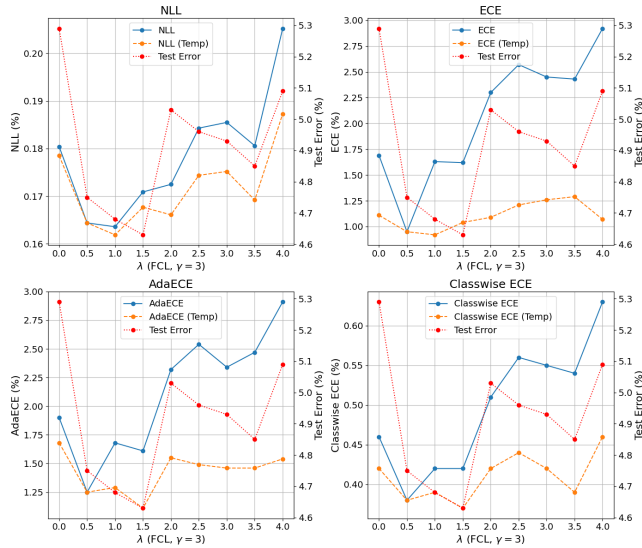
6 RELATED WORK

Improving the calibration of deep neural networks (DNNs) is critical for reliable uncertainty estimation. A common strategy involves post-hoc calibration methods, which adjust a pre-trained model’s output probabilities without altering its architecture or training procedure. Platt scaling [38], originally designed for binary classifiers,

⁴The Focal Calibration Loss reduces to the standard focal loss when $\lambda = 0$.

Table 4: Robustness on OoD Dataset Shift. \uparrow AUROC (%) for shifting CIFAR-10 (in-distribution) to SVHN and CIFAR-10-C (OoD).

Dataset	Model	Weight Decay[12]		Brier Loss[5]		MMCE[22]		Label Smooth[43]		Focal Loss - 53[32]		Dual Focal[44]		Focal Calibration	
		Pre T	Post T	Pre T	Post T	Pre T	Post T	Pre T	Post T	Pre T	Post T	Pre T	Post T	Pre T	Post T
CIFAR-10/SVHN	ResNet-50	91.53	91.95	95.11	95.26	75.73	75.19	85.07	85.08	90.72	90.72	93.54	93.82	92.28	92.28
	ResNet-110	77.56	76.11	94.49	94.67	75.01	73.40	82.94	83.03	90.11	90.18	95.26	95.69	92.60	92.60
	Wide-ResNet-26-10	87.12	87.25	92.75	92.75	93.31	93.07	88.39	88.42	93.45	93.47	92.63	92.60	95.77	95.77
	DenseNet-121	92.93	91.57	95.62	95.62	90.42	89.34	74.43	74.88	93.01	92.95	93.93	93.99	96.20	96.20
CIFAR-10/CIFAR-10-C	ResNet-50	83.09	81.29	89.91	89.89	87.81	88.13	67.98	68.34	91.37	91.37	87.79	87.64	89.66	89.66
	ResNet-110	74.89	71.87	77.11	76.58	73.57	72.62	65.26	65.58	78.46	77.90	83.35	82.54	89.88	89.88
	Wide-ResNet-26-10	80.67	79.79	89.44	89.44	76.80	76.34	84.43	84.47	82.91	83.51	84.05	83.89	90.98	90.98
	DenseNet-121	86.96	80.91	53.87	53.87	69.15	65.23	72.26	72.55	90.35	90.51	82.90	82.32	90.57	90.57

**Figure 5: Different hyperparameters trained on CIFAR-10 with ResNet-110. The plots show the performance of the FCL with varying calibration parameter λ ($\gamma = 3.0$) across different metrics: NLL, ECE, AdaECE, and Classwise-ECE. Each plot includes before (blue solid lines) and after (orange dashed lines) temperature scaling, alongside the Test Error (red dotted lines) ⁴.**

was extended to multi-class settings by applying a linear transformation to logits to improve calibration. More recent methods like Temperature Scaling [12] introduce a temperature parameter to adjust the predicted logits, effectively reducing the Expected Calibration Error (ECE) across various models. Histogram Binning [52] discretizes the probability space into bins to align confidence scores with empirical frequencies. While effective, these methods require held-out validation data and assume the test distribution matches the calibration data.

6.1 Calibration Strategies

Regularization-based approaches aim to improve calibration during training. Label Smoothing [34, 43] mitigates overconfidence by blending true labels with a uniform distribution, softening hard targets to enhance generalization and uncertainty estimation. Additionally, auxiliary losses like the Maximum Mean Calibration Error

(MMCE) [22] explicitly minimize the difference between predicted and actual confidence levels. Bayesian techniques offer a principled way to quantify uncertainty. For instance, Deep Ensembles [23] aggregate predictions from multiple independently trained models to yield well-calibrated confidence estimates, though they are computationally intensive and less practical in resource-limited settings. Focal Loss [28], designed to handle class imbalance in object detection, also affects calibration by concentrating on hard-to-classify examples, which can reduce overconfidence but sometimes result in underconfident predictions [9]. Dual Focal Loss (DFL) [44] improves upon this by maximizing the margin between the true class logit and the next highest logit, balancing overconfidence and underconfidence to enhance calibration. Recently, smoothing-based methods have been introduced to provide continuous calibration measures. The Smooth Calibration Error (smCE) [4] uses kernel-based smoothing to create a differentiable measure of calibration error, overcoming the limitations of discrete binning in traditional ECE calculations.

6.2 Calibration in Transformers and LLMs

Calibration of transformer-based language models has been evaluated across various natural language processing tasks, including machine translation [21], question answering [18], and selective prediction [29, 48]. Recently, with the growing prominence of large-scale generative language models (LLMs), studies have begun to examine their calibration properties [17, 20, 27, 46, 50] and zero-shot/few-shot learning [6]. To enhance text generation quality and improve models' handling of ambiguity, more studies have focused on addressing miscalibration of token-level probabilities by implementing calibration techniques that enable models to express uncertainty more accurately [21, 27, 30, 51, 56].

7 CONCLUSIONS

In conclusion, our FCL effectively addresses the limitations of traditional Focal Loss by integrating a calibration term that significantly enhances the accuracy of probability estimations. Traditional Focal Loss has been instrumental in reducing misclassification rates by focusing on hard-to-classify samples; however, it often falls short in providing well-calibrated predictions. By ensuring that the loss function is strictly proper, FCL delivers more reliable class-posterior probabilities, which directly contributes to improved model confidence and reliability across various applications even in unforeseen circumstances.

REFERENCES

- [1] Josh Achiam, Steven Adler, Sandhini Agarwal, Lama Ahmad, Ilge Akkaya, Florencia Leoni Aleman, Diogo Almeida, Janko Altmenschmidt, Sam Altman, Shyamal Anadkat, et al. 2023. Gpt-4 technical report. *arXiv* (2023).
- [2] Peter L Bartlett, Michael I Jordan, and Jon D McAuliffe. 2006. Convexity, classification, and risk bounds. *J. Amer. Statist. Assoc.* 101, 473 (2006), 138–156.
- [3] Jaroslaw Blasiok, Parikshit Gopalan, Lunjia Hu, and Preetum Nakkiran. 2024. When does optimizing a proper loss yield calibration? *Advances in Neural Information Processing Systems* 36 (2024).
- [4] Jaroslaw Blasiok and Preetum Nakkiran. 2023. Smooth ECE: Principled reliability diagrams via kernel smoothing. *arXiv preprint arXiv:2309.12236* (2023).
- [5] Glenn W. Brier. 1950. Verification of forecasts expressed in terms of probability. *Monthly weather review* 78, 1 (1950), 1–3.
- [6] Tom B Brown. 2020. Language models are few-shot learners. *arXiv preprint arXiv:2005.14165* (2020).
- [7] Andreas Buja, Werner Stuetzle, and Yi Shen. 2005. Loss functions for binary class probability estimation and classification: Structure and applications. *Working draft, November 3* (2005), 13.
- [8] Blasiok, Jaroslaw and Nakkiran, Preetum. 2024. ml-calibration. <https://github.com/apple/ml-calibration>. Accessed: 2024-10-08.
- [9] Nontawat Charoenphakdee, Jayakorn Vongkulbhisal, Nuttapon Chairatanakul, and Masashi Sugiyama. 2021. On focal loss for class-posterior probability estimation: A theoretical perspective. In *IEEE/CVF. 5202–5211*.
- [10] J. Deng, W. Dong, R. Socher, L. Li, K. Li, and F. Li. 2009. ImageNet: A Large-Scale Hierarchical Image Database. *2009 IEEE Conference on Computer Vision and Pattern Recognition* (2009), 248–255. <https://doi.org/10.1109/CVPR.2009.5206848>
- [11] Tilmann Gneiting and Adrian E Raftery. 2007. Strictly proper scoring rules, prediction, and estimation. *Journal of the American statistical Association* 102, 477 (2007), 359–378.
- [12] Chuan Guo, Geoff Pleiss, Yu Sun, and Kilian Q. Weinberger. 2017. On calibration of modern neural networks. In *International conference on machine learning*. PMLR, 1321–1330.
- [13] Kaiming He, Xiangyu Zhang, Shaoqing Ren, and Jian Sun. 2016. Deep Residual Learning for Image Recognition. *2016 IEEE Conference on Computer Vision and Pattern Recognition (CVPR)* (2016), 770–778.
- [14] Kaiming He, Xiangyu Zhang, Shaoqing Ren, and Jian Sun. 2016. Identity Mappings in Deep Residual Networks. *European Conference on Computer Vision (ECCV)* (2016), 630–645. https://doi.org/10.1007/978-3-319-46493-0_38
- [15] Dan Hendrycks and Thomas Dietterich. 2019. Benchmarking Neural Network Robustness to Common Corruptions and Perturbations. *Proceedings of the International Conference on Learning Representations (ICLR)* (2019). <https://arxiv.org/abs/1903.12261>
- [16] Gao Huang, Zhuang Liu, Laurens van der Maaten, and Kilian Q. Weinberger. 2017. Densely Connected Convolutional Networks. *2017 IEEE Conference on Computer Vision and Pattern Recognition (CVPR)* (2017), 2261–2269. <https://doi.org/10.1109/CVPR.2017.243>
- [17] Yukun Huang, Yixin Liu, Raghuveer Thirukovalluru, Arman Cohan, and Bhuwan Dhingra. 2024. Calibrating Long-form Generations from Large Language Models. *arXiv preprint arXiv:2402.06544* (2024).
- [18] Zhengbao Jiang, Frank F Xu, Jun Araki, and Graham Neubig. 2020. How can we know what language models know? *Transactions of the Association for Computational Linguistics* 8 (2020), 423–438.
- [19] Alex Krizhevsky. 2009. Learning Multiple Layers of Features from Tiny Images. (2009). <https://www.cs.toronto.edu/~kriz/cifar.html> Technical report.
- [20] Lorenz Kuhn, Yarin Gal, and Sebastian Farquhar. 2023. Semantic uncertainty: Linguistic invariances for uncertainty estimation in natural language generation. *arXiv preprint arXiv:2302.09664* (2023).
- [21] Aviral Kumar and Sunita Sarawagi. 2019. Calibration of encoder decoder models for neural machine translation. *arXiv preprint arXiv:1903.00802* (2019).
- [22] Aviral Kumar, Sunita Sarawagi, and Ujjwal Jain. 2018. Trainable calibration measures for neural networks from kernel mean embeddings. In *International Conference on Machine Learning*. PMLR, 2805–2814.
- [23] Balaji Lakshminarayanan, Alexander Pritzel, and Charles Blundell. 2017. Simple and scalable predictive uncertainty estimation using deep ensembles. *Advances in neural information processing systems* 30 (2017).
- [24] Ken Lang. 1995. NewsWeeder: Learning to Filter Netnews. In *Proceedings of the 12th International Conference on Machine Learning*, 331–339.
- [25] Wenhao Liang, Zhengyang Li, and Weitong Chen. 2024. Enhancing Financial Market Predictions: Causality-Driven Feature Selection. In *Advanced Data Mining and Applications*. Springer.
- [26] Min Lin, Qiang Chen, and Shuicheng Yan. 2014. Network In Network. In *Proceedings of the International Conference on Learning Representations (ICLR)*.
- [27] Stephanie Lin, Jacob Hilton, and Owain Evans. 2022. Teaching models to express their uncertainty in words. *arXiv preprint arXiv:2205.14334* (2022).
- [28] Tsung-Yi Lin, Priya Goyal, Ross Girshick, Kaiming He, and Piotr Dollár. 2017. Focal Loss for Dense Object Detection. In *Proceedings of the IEEE International Conference on Computer Vision (ICCV)*. 2980–2988.
- [29] Yu Lu, Jiali Zeng, Jiajun Zhang, Shuangzhi Wu, and Mu Li. 2022. Learning confidence for transformer-based neural machine translation. *arXiv preprint arXiv:2203.11413* (2022).
- [30] Sabrina J Mielke, Arthur Szlam, Emily Dinan, and Y-Lan Boureau. 2022. Reducing conversational agents’ overconfidence through linguistic calibration. *Transactions of the Association for Computational Linguistics* 10 (2022), 857–872.
- [31] Matthias Minderer, Josip Djolonga, Rob Romijnders, Frances Hubis, Xiaohua Zhai, Neil Houlsby, Dustin Tran, and Mario Lucic. 2021. Revisiting the calibration of modern neural networks. *Advances in Neural Information Processing Systems* 34 (2021), 15682–15694.
- [32] Jishnu Mukhoti, Viveka Kulharia, Amartya Sanyal, Stuart Golodetz, Philip Torr, and Puneet Dokania. 2020. Calibrating deep neural networks using focal loss. *Advances in Neural Information Processing Systems* 33 (2020), 15288–15299.
- [33] Jishnu Mukhoti, Viveka Kulharia, Amartya Sanyal, Stuart Golodetz, Philip HS Torr, and Puneet K Dokania. 2020. Focal Calibration. https://github.com/torrvision/focal_calibration. Accessed: 2024-10-08.
- [34] Rafael Müller, Simon Kornblith, and Geoffrey E. Hinton. 2019. When does label smoothing help? *Advances in neural information processing systems* 32 (2019).
- [35] Yuval Netzer, Tao Wang, Adam Coates, Alessandro Bissacco, Bo Wu, and Andrew Y Ng. 2011. Reading Digits in Natural Images with Unsupervised Feature Learning. (2011). <http://ufldl.stanford.edu/housenumbers>
- [36] Andrew Y Ng. 2004. Feature selection, L 1 vs. L 2 regularization, and rotational invariance. In *Proceedings of the twenty-first international conference on Machine learning*, 78.
- [37] Alexandru Niculescu-Mizil and Rich Caruana. 2005. Predicting good probabilities with supervised learning. In *Proceedings of the 22nd icml*. 625–632.
- [38] John Platt et al. 1999. Probabilistic outputs for support vector machines and comparisons to regularized likelihood methods. *Advances in large margin classifiers* 10, 3 (1999), 61–74.
- [39] Pranav Rajpurkar, Jeremy Irvin, Kaylie Zhu, Brandon Yang, Hershel Mehta, Tony Duan, Daisy Ding, Aarti Bagul, Curtis Langlotz, Katie Shpanskaya, Matthew P. Lungren, and Andrew Y. Ng. 2017. CheXNet: Radiologist-Level Pneumonia Detection on Chest X-Rays with Deep Learning. *arXiv preprint arXiv:1711.05225* (2017). <https://arxiv.org/abs/1711.05225>
- [40] Mark D Reid and Robert C Williamson. 2010. Composite binary losses. *The Journal of Machine Learning Research* 11 (2010), 2387–2422.
- [41] Ramprasaath R. Selvaraju, Michael Cogswell, Abhishek Das, Ramakrishna Vedantam, Devi Parikh, and Dhruv Batra. 2017. Grad-cam: Visual explanations from deep networks via gradient-based localization. In *Proceedings of the IEEE international conference on computer vision*. 618–626.
- [42] Emir H Shuford Jr, Arthur Albert, and H Edward Massengill. 1966. Admissible probability measurement procedures. *Psychometrika* 31, 2 (1966), 125–145.
- [43] Christian Szegedy, Vincent Vanhoucke, Sergey Ioffe, Jon Shlens, and Zbigniew Wojna. 2016. Rethinking the inception architecture for computer vision. In *cvpr*.
- [44] Linwei Tao, Mingjing Dong, and Chang Xu. 2023. Dual Focal Loss for Calibration. In *International Conference on Machine Learning (ICML)*.
- [45] Ambuj Tewari and Peter L Bartlett. 2007. On the Consistency of Multiclass Classification Methods. *Journal of Machine Learning Research* 8, 5 (2007).
- [46] Katherine Tian, Eric Mitchell, Allan Zhou, Archit Sharma, Rafael Rafailov, Huaxiu Yao, Chelsea Finn, and Christopher D Manning. 2023. Just ask for calibration: Strategies for eliciting calibrated confidence scores from language models fine-tuned with human feedback. *arXiv preprint arXiv:2305.14975* (2023).
- [47] Vladimir Naumovich Vapnik, Vladimir Vapnik, et al. 1998. Statistical learning theory. (1998).
- [48] Neeraj Varshney, Swaroop Mishra, and Chitta Baral. 2022. Investigating Selective Prediction Approaches Across Several Tasks in IID, OOD, and Adversarial Settings. In *Findings of the Association for Computational Linguistics: ACL 2022*, Smaranda Muresan, Preslav Nakov, and Aline Villavicencio (Eds.). Association for Computational Linguistics, Dublin, Ireland, 1995–2002. <https://doi.org/10.18653/v1/2022.findings-acl.158>
- [49] Robert C Williamson, Elodie Vernet, and Mark D Reid. 2016. Composite multiclass losses. *Journal of Machine Learning Research* 17, 222 (2016), 1–52.
- [50] Miao Xiong, Zhiyuan Hu, Xinyang Lu, Yifei Li, Jie Fu, Junxian He, and Bryan Hooi. 2023. Can llms express their uncertainty? an empirical evaluation of confidence elicitation in llms. *arXiv preprint arXiv:2306.13063* (2023).
- [51] Benfeng Xu, Quan Wang, Zhendong Mao, Yajuan Lyu, Qiaoqiao She, and Yongdong Zhang. 2023. k NN prompting: Beyond-context learning with calibration-free nearest neighbor inference. *arXiv preprint arXiv:2303.13824* (2023).
- [52] Bianca Zadrozny and Charles Elkan. 2002. Transforming Classifier Scores into Accurate Multiclass Probability Estimates. In *Proceedings of the ACM SIGKDD International Conference on Knowledge Discovery and Data Mining*, 694–699.
- [53] Sergey Zagoruyko and Nikos Komodakis. 2016. Wide Residual Networks. *Proceedings of the British Machine Vision Conference (BMVC)* (2016). <https://arxiv.org/abs/1605.07146>
- [54] Tong Zhang. 2004. Statistical analysis of some multi-category large margin classification methods. *Journal of Machine Learning Research* 5, Oct (2004).

- [55] Xiang Zhang, Junbo Zhao, and Yann LeCun. 2015. Character-level convolutional networks for text classification. *Advances in neural information processing systems* 28 (2015).
- [56] Kaitlyn Zhou, Dan Jurafsky, and Tatsunori Hashimoto. 2023. Navigating the grey area: How expressions of uncertainty and overconfidence affect language models. *arXiv preprint arXiv:2302.13439* (2023).

A APPENDIX

A.1 Evaluation Metrics

Formally, the ECE can be approximated by grouping predictions into M bins and calculating the average confidence and accuracy for each bin:

$$\text{ECE} = \sum_{m=1}^M \frac{|B_m|}{N} |\text{acc}(B_m) - \text{conf}(B_m)| \quad (18)$$

where N is the total number of samples, M is the number of bins, B_m is the set of indices of samples whose predicted probability falls into the m -th bin, $|B_m|$ is the number of samples in bin B_m , $\text{acc}(B_m)$ is the accuracy of the samples in bin B_m , and $\text{conf}(B_m)$ is the average confidence of the samples in bin B_m defined in Eq. (19).

$$\text{acc}(B_m) = \frac{1}{|B_m|} \sum_{i \in B_m} \mathbf{1}(\hat{y}_i = y_i), \quad \text{conf}(B_m) = \frac{1}{|B_m|} \sum_{i \in B_m} \hat{p}_i \quad (19)$$

$$\text{MCE} = \max_{m \in \{1, \dots, M\}} |\text{acc}(B_m) - \text{conf}(B_m)| \quad (20)$$

$$\text{AdaECE} = \sum_{m=1}^M \frac{|B_m|}{N} |\text{acc}(B_m) - \text{conf}(B_m)| \quad (21)$$

$$\text{ClasswiseECE} = \frac{1}{K} \sum_{k=1}^K \sum_{m=1}^M \frac{|B_{km}|}{N_k} |\text{acc}(B_{km}) - \text{conf}(B_{km})| \quad (22)$$

where N_k is the number of samples in class k , B_{km} is the set of indices of samples of class k whose predicted probability falls into the m -th bin, $|B_{km}|$ is the number of samples in bin B_{km} , $\text{acc}(B_{km})$ is the accuracy of the samples in bin B_{km} , and $\text{conf}(B_{km})$ is the average confidence of the samples in bin B_{km} .

A.2 Proof of Thm. 6 Focal Calibration Loss mitigates overconfidence (OC) and underconfidence (UC)

In this appendix, we provide a mathematical proof that minimizing the Focal Calibration Loss $\mathcal{L}_{\text{FCL}}^{\gamma, \lambda}$ mitigates overconfidence (OC) and underconfidence (UC) in the predicted probabilities of a classifier.

Step 1: Bounding Overconfidence and Underconfidence. We aim to bound the difference between the maximum predicted probability and the maximum true class probability. For any $\mathbf{x} \in \mathcal{X}$, we have:

$$\left| \max_k \hat{p}_k(\mathbf{x}) - \max_k \eta_k(\mathbf{x}) \right| \leq \|\hat{\mathbf{p}}(\mathbf{x}) - \boldsymbol{\eta}(\mathbf{x})\|_{\infty}, \quad (23)$$

where $\|\cdot\|_{\infty}$ denotes the infinity norm.

PROOF. Let $k^* = \arg \max_k \hat{p}_k(\mathbf{x})$ and $k^\dagger = \arg \max_k \eta_k(\mathbf{x})$. Then,

$$\left| \max_k \hat{p}_k(\mathbf{x}) - \max_k \eta_k(\mathbf{x}) \right| = |\hat{p}_{k^*}(\mathbf{x}) - \eta_{k^\dagger}(\mathbf{x})|. \quad (24)$$

Using the triangle inequality, we have:

$$|\hat{p}_{k^*}(\mathbf{x}) - \eta_{k^\dagger}(\mathbf{x})| \leq |\hat{p}_{k^*}(\mathbf{x}) - \eta_{k^*}(\mathbf{x})| + |\eta_{k^*}(\mathbf{x}) - \eta_{k^\dagger}(\mathbf{x})|. \quad (25)$$

Since $\eta_{k^\dagger}(\mathbf{x}) \geq \eta_{k^*}(\mathbf{x})$ by the definition of k^\dagger and k^* , it follows that:

$$|\eta_{k^*}(\mathbf{x}) - \eta_{k^\dagger}(\mathbf{x})| = \eta_{k^\dagger}(\mathbf{x}) - \eta_{k^*}(\mathbf{x}) \geq 0. \quad (26)$$

Similarly, since $\hat{p}_{k^*}(\mathbf{x}) \geq \hat{p}_{k^\dagger}(\mathbf{x})$, we have:

$$\hat{p}_{k^*}(\mathbf{x}) - \hat{p}_{k^\dagger}(\mathbf{x}) \geq 0. \quad (27)$$

Combining Equations (25) and (26), we get:

$$|\hat{p}_{k^*}(\mathbf{x}) - \eta_{k^\dagger}(\mathbf{x})| \leq |\hat{p}_{k^*}(\mathbf{x}) - \eta_{k^*}(\mathbf{x})| + (\eta_{k^\dagger}(\mathbf{x}) - \eta_{k^*}(\mathbf{x})). \quad (28)$$

Since $\eta_{k^\dagger}(\mathbf{x}) - \eta_{k^*}(\mathbf{x}) \leq \max_k |\eta_k(\mathbf{x}) - \eta_k(\mathbf{x})| = 0$, the second term is zero. Therefore,

$$|\hat{p}_{k^*}(\mathbf{x}) - \eta_{k^\dagger}(\mathbf{x})| \leq |\hat{p}_{k^*}(\mathbf{x}) - \eta_{k^*}(\mathbf{x})|. \quad (29)$$

Thus,

$$\left| \max_k \hat{p}_k(\mathbf{x}) - \max_k \eta_k(\mathbf{x}) \right| \leq \max_k |\hat{p}_k(\mathbf{x}) - \eta_k(\mathbf{x})| = \|\hat{\mathbf{p}}(\mathbf{x}) - \boldsymbol{\eta}(\mathbf{x})\|_{\infty}. \quad (30)$$

□

Step 2: Relating Infinity Norm to Euclidean Norm. We have the relationship between norms:

$$\|\hat{\mathbf{p}}(\mathbf{x}) - \boldsymbol{\eta}(\mathbf{x})\|_{\infty} \leq \|\hat{\mathbf{p}}(\mathbf{x}) - \boldsymbol{\eta}(\mathbf{x})\|_2. \quad (31)$$

This follows because the infinity norm is less than or equal to the Euclidean norm.

Step 3: Combining Steps 1 and 2. From inequalities (23) and (31), we obtain:

$$\left| \max_k \hat{p}_k(\mathbf{x}) - \max_k \eta_k(\mathbf{x}) \right| \leq \|\hat{\mathbf{p}}(\mathbf{x}) - \boldsymbol{\eta}(\mathbf{x})\|_2. \quad (32)$$

Step 4: Minimizing the Calibration Loss Reduces the Norm. The calibration loss for a single data point is:

$$\mathcal{L}_{\text{calib}}(f(\mathbf{x}), \mathbf{y}) = \|\hat{\mathbf{p}}(\mathbf{x}) - \mathbf{y}\|_2^2. \quad (33)$$

Since \mathbf{y} is a one-hot encoding sampled from the distribution $\boldsymbol{\eta}(\mathbf{x})$, we have:

$$\mathbb{E}_{\mathbf{y} \sim \boldsymbol{\eta}(\mathbf{x})} [\|\hat{\mathbf{p}}(\mathbf{x}) - \mathbf{y}\|_2^2] = \|\hat{\mathbf{p}}(\mathbf{x}) - \boldsymbol{\eta}(\mathbf{x})\|_2^2 + \sum_{k=1}^K \eta_k(\mathbf{x})(1 - \eta_k(\mathbf{x})). \quad (34)$$

The term $\sum_{k=1}^K \eta_k(\mathbf{x})(1 - \eta_k(\mathbf{x}))$ is independent of $\hat{\mathbf{p}}(\mathbf{x})$ and represents the intrinsic uncertainty of the true distribution. Therefore, minimizing $\mathcal{L}_{\text{calib}}$ effectively minimizes $\|\hat{\mathbf{p}}(\mathbf{x}) - \boldsymbol{\eta}(\mathbf{x})\|_2^2$.

Step 5: Impact on Overconfidence and Underconfidence. By minimizing $\|\hat{\mathbf{p}}(\mathbf{x}) - \boldsymbol{\eta}(\mathbf{x})\|_2^2$, we directly reduce the bound in Equation (32) on $|\max_k \hat{p}_k(\mathbf{x}) - \max_k \eta_k(\mathbf{x})|$. This means that the difference between the highest predicted probability and the highest true probability decreases, mitigating both overconfidence and underconfidence.

Minimizing the Focal Calibration Loss $\mathcal{L}_{\text{FCL}}^{\gamma, \lambda}$ includes minimizing the calibration loss component $\mathcal{L}_{\text{calib}}$, which reduces the Euclidean distance between the predicted probabilities $\hat{\mathbf{p}}(\mathbf{x})$ and the true class-posterior probabilities $\boldsymbol{\eta}(\mathbf{x})$. This, in turn, reduces the bound on the difference between the maximum predicted probability and the maximum true probability, thereby mitigating overconfidence and underconfidence.

A.3 Proof that Minimizing the Focal Calibration Loss Recovers the True Class-Posterior Probabilities

PROOF. Let \mathcal{X} be the input space and $\mathcal{Y} = \{1, 2, \dots, K\}$ the set of K classes. For a given input $\mathbf{x} \in \mathcal{X}$, let $\boldsymbol{\eta} = [\eta_1, \eta_2, \dots, \eta_K]^\top$ denote the true class-posterior probabilities, where $\eta_i = \mathbb{P}(y = i | \mathbf{x})$ and $\sum_{i=1}^K \eta_i = 1$; $\mathbf{q} = [q_1, q_2, \dots, q_K]^\top$ be the predicted probability vector, where $q_i \in (0, 1)$ and $\sum_{i=1}^K q_i = 1$. We aim to minimize the Focal Calibration Loss (FCL) and Our goal is to show that the minimizer \mathbf{q}^* of $\mathcal{L}_{\text{FCL}}^{\gamma, \lambda}(\mathbf{q})$ satisfies $q_i^* = \eta_i$ for all i .

$$\mathcal{L}_{\text{FCL}}^{\gamma, \lambda}(\mathbf{q}) = - \sum_{i=1}^K \eta_i (1 - q_i)^\gamma \log q_i + \lambda \sum_{i=1}^K (q_i - \eta_i)^2, \quad (35)$$

subject to $q_i > 0$ and $\sum_{i=1}^K q_i = 1$.

Step 1: Convexity of the Loss Function. Before proceeding, we establish that $\mathcal{L}_{\text{FCL}}^{\gamma, \lambda}(\mathbf{q})$ is strictly convex in \mathbf{q} over the domain $q_i \in (0, 1)$.

- Calibration Loss Term: The term $\lambda \sum_{i=1}^K (q_i - \eta_i)^2$ is strictly convex in \mathbf{q} because it is a sum of squared terms.
- Focal Loss Term: The term $-\sum_{i=1}^K \eta_i (1 - q_i)^\gamma \log q_i$ is convex in q_i for $q_i \in (0, 1)$. The function $\phi(q_i) = -(1 - q_i)^\gamma \log q_i$ is convex in $q_i \in (0, 1)$ for $\gamma \geq 0$. Since $\eta_i \geq 0$, and a non-negative weighted sum of convex functions is convex, the focal loss term is convex.

The sum of a strictly convex function (calibration loss) and a convex function (focal loss) is strictly convex (See Thm. 14 in Appendix A.4). Therefore, $\mathcal{L}_{\text{FCL}}^{\gamma, \lambda}(\mathbf{q})$ is strictly convex in \mathbf{q} .

Step 2: Existence and Uniqueness of the Minimizer. Because $\mathcal{L}_{\text{FCL}}^{\gamma, \lambda}(\mathbf{q})$ is strictly convex and the feasible set defined by $q_i > 0$ and $\sum_{i=1}^K q_i = 1$ is convex and closed, there exists a unique global minimizer \mathbf{q}^* .

Step 3: Setting Up the Lagrangian. To find the minimizer, we set up the Lagrangian function incorporating the equality constraint:

$$\mathcal{L}(\mathbf{q}, \mu) = - \sum_{i=1}^K \eta_i (1 - q_i)^\gamma \log q_i + \lambda \sum_{i=1}^K (q_i - \eta_i)^2 + \mu \left(\sum_{i=1}^K q_i - 1 \right). \quad (36)$$

We do not need to include inequality constraints $q_i > 0$ explicitly because $q_i \in (0, 1)$ due to the logarithm and the domain of \mathbf{q} .

Step 4: Deriving the KKT Conditions. The Karush-Kuhn-Tucker (KKT) conditions for optimality are:

- (1) Stationarity: For each i , $\frac{\partial \mathcal{L}}{\partial q_i} = 0$.
- (2) Primal Feasibility: $\sum_{i=1}^K q_i = 1$.
- (3) Dual Feasibility: Not applicable here since there are no inequality constraints in q_i after considering the domain.
- (4) Complementary Slackness: Not applicable since we don't have inequality constraints with slack variables.

Compute the partial derivative:

$$\frac{\partial \mathcal{L}}{\partial q_i} = \eta_i \left[\gamma (1 - q_i)^{\gamma-1} \log q_i + \frac{(1 - q_i)^\gamma}{q_i} \right] + 2\lambda (q_i - \eta_i) + \mu = 0. \quad (37)$$

Step 5: Analyzing the Stationarity Condition. Let's denote:

$$S_i(q_i) = \eta_i \left[\gamma (1 - q_i)^{\gamma-1} \log q_i + \frac{(1 - q_i)^\gamma}{q_i} \right] + 2\lambda (q_i - \eta_i). \quad (38)$$

Then the stationarity condition becomes: $S_i(q_i) + \mu = 0$. Since μ is the same for all i , we have:

$$S_i(q_i) = S_j(q_j) \quad \forall i, j. \quad (39)$$

Step 6: Showing that $q_i^ = \eta_i$ satisfies the conditions.* We need evaluate $S_i(q_i)$ at $q_i = \eta_i$:

1. When $\eta_i > 0$ and $\eta_i \in (0, 1)$: Compute $\log \eta_i$, $(1 - \eta_i)$, and γ . Substitute $q_i = \eta_i$ into $S_i(q_i)$:

$$S_i(\eta_i) = \eta_i \left[\gamma (1 - \eta_i)^{\gamma-1} \log \eta_i + \frac{(1 - \eta_i)^\gamma}{\eta_i} \right] + 2\lambda (\eta_i - \eta_i) \quad (40)$$

$$= \eta_i \left[\gamma (1 - \eta_i)^{\gamma-1} \log \eta_i + \frac{(1 - \eta_i)^\gamma}{\eta_i} \right]. \quad (41)$$

2. Observation: The term $S_i(\eta_i)$ depends only on η_i and is constant for each i . Therefore, $S_i(\eta_i) + \mu = 0$ holds for each i with the same μ .

3. Equality Across Classes: Since $S_i(\eta_i) + \mu = 0$ for all i , and $S_i(\eta_i)$ is a constant for each i , the only way this can hold is if $\eta_i = \eta_j$ or the terms are adjusted by λ .

However, this suggests that $q_i = \eta_i$ satisfies the stationarity condition for some μ , but we need to ensure that this solution indeed minimizes the loss function.

Step 7: Uniqueness and Minimization. Since $\mathcal{L}_{\text{FCL}}^{\gamma, \lambda}(\mathbf{q})$ is strictly convex, any stationary point is the unique global minimizer. Let's evaluate $\mathcal{L}_{\text{FCL}}^{\gamma, \lambda}(\mathbf{q})$ at $\mathbf{q} = \boldsymbol{\eta}$:

1. Calibration Loss term is minimized to 0: $\lambda \sum_{i=1}^K (\eta_i - \eta_i)^2 = 0$.
2. Focal Loss term $-\sum_{i=1}^K \eta_i (1 - \eta_i)^\gamma \log \eta_i$ is minimized when $q_i = \eta_i$ because the negative log-likelihood is minimized when the predicted probabilities match the true probabilities.

Since $\mathbf{q} = \boldsymbol{\eta}$ yields the minimal possible value of $\mathcal{L}_{\text{FCL}}^{\gamma, \lambda}(\mathbf{q})$, and the loss function is strictly convex, $\mathbf{q}^* = \boldsymbol{\eta}$ is the unique global minimizer.

Step 8: Handling the case when $\eta_i = 0$ or $\eta_i = 1$. 1. If $\eta_i = 0$: The focal loss term for class i becomes zero: $-\eta_i (1 - q_i)^\gamma \log q_i = 0$. The calibration loss term is $\lambda (q_i - 0)^2 = \lambda q_i^2$, minimized when $q_i = 0$.

2. If $\eta_i = 1$: The focal loss term becomes: $-(1 - q_i)^\gamma \log q_i$. This is minimized when $q_i = 1$. The calibration loss term $\lambda (q_i - 1)^2$ is minimized when $q_i = 1$.

In both cases, $q_i^* = \eta_i$ minimizes the loss.

Therefore, minimizing the Focal Calibration Loss $\mathcal{L}_{\text{FCL}}^{\gamma, \lambda}(\mathbf{q})$ over the probability simplex recovers the true class-posterior probabilities $\mathbf{q}^* = \boldsymbol{\eta}$. \square

A.4 Convexity of the Sum of Strictly Convex and Convex Functions

THEOREM 14. *Let $f : \mathbb{R}^n \rightarrow \mathbb{R}$ be a strictly convex function, and let $g : \mathbb{R}^n \rightarrow \mathbb{R}$ be a convex function. Then the function $h = f + g$ is strictly convex on \mathbb{R}^n .*

PROOF. Let $x, y \in \mathbb{R}^n$ with $x \neq y$, and let $\theta \in (0, 1)$. Since f is strictly convex, we have:

$$f(\theta x + (1 - \theta)y) < \theta f(x) + (1 - \theta)f(y). \quad (42)$$

Similarly, since g is convex, we have:

$$g(\theta x + (1 - \theta)y) \leq \theta g(x) + (1 - \theta)g(y). \quad (43)$$

Adding the two inequalities, we obtain:

$$\begin{aligned} h(\theta x + (1 - \theta)y) &= f(\theta x + (1 - \theta)y) + g(\theta x + (1 - \theta)y) \\ &< \theta f(x) + (1 - \theta)f(y) + \theta g(x) + (1 - \theta)g(y) \\ &= \theta(f(x) + g(x)) + (1 - \theta)(f(y) + g(y)) \\ &= \theta h(x) + (1 - \theta)h(y). \end{aligned} \quad (44)$$

This strict inequality shows that h is strictly convex on \mathbb{R}^n . \square

A.5 Proof that the Focal Calibration Loss Satisfies the Strictly Order-Preserving Property

THEOREM 15. *The Focal Calibration Loss $\mathcal{L}_{\text{FCL}}^{\gamma, \lambda}$ is classification-calibrated; that is, it satisfies the Strictly Order-Preserving Property.*

PROOF. From Def. 9, we aim to show that the Focal Calibration Loss (FCL) satisfies:

$$q_i^* < q_j^* \Rightarrow \eta_i < \eta_j, \quad (45)$$

where $\mathbf{q}^* = [q_1^*, q_2^*, \dots, q_K^*]^\top$ is the minimizer of the pointwise conditional risk $\mathcal{R}^{\mathcal{L}_{\text{FCL}}}(\mathbf{q})$.

Step 1: Define the Focal Calibration Loss (FCL). The Focal Calibration Loss for a single sample \mathbf{x} with true label $y \in \{1, 2, \dots, K\}$ is defined as:

$$\mathcal{L}_{\text{FCL}}^{\gamma, \lambda}(\mathbf{q}, y) = -(1 - q_y)^\gamma \log q_y + \lambda \sum_{i=1}^K (q_i - \eta_i)^2, \quad (46)$$

where:

- $\mathbf{q} = [q_1, q_2, \dots, q_K]^\top$ is the predicted probability distribution over the K classes.
- $\eta_i = \mathbb{P}(y = i \mid \mathbf{x})$ is the true class-posterior probability for class i .
- $\gamma \geq 0$ is the focusing parameter.
- $\lambda > 0$ is the calibration coefficient.

Step 2: Define the Pointwise Conditional Risk. The pointwise conditional risk $\mathcal{R}^{\mathcal{L}}(\mathbf{q})$ for the loss function \mathcal{L} is defined as:

$$\mathcal{R}^{\mathcal{L}}(\mathbf{q}) = \mathbb{E}_{y|\mathbf{x}}[\mathcal{L}(\mathbf{q}, y)] = \sum_{i=1}^K \eta_i \mathcal{L}(\mathbf{q}, i). \quad (47)$$

For FCL, this becomes:

$$\mathcal{R}^{\mathcal{L}_{\text{FCL}}}(\mathbf{q}) = \sum_{i=1}^K \eta_i [-(1 - q_i)^\gamma \log q_i] + \lambda \sum_{i=1}^K (q_i - \eta_i)^2. \quad (48)$$

Step 3: Find the Minimizer of the Pointwise Conditional Risk. Our objective is to find the minimizer \mathbf{q}^* of $\mathcal{R}^{\mathcal{L}_{\text{FCL}}}(\mathbf{q})$:

$$\mathbf{q}^* = \arg \min_{\mathbf{q}} \left\{ \mathcal{R}^{\mathcal{L}_{\text{FCL}}}(\mathbf{q}) \mid \sum_{i=1}^K q_i = 1, \quad q_i > 0 \quad \forall i \right\}. \quad (49)$$

Step 4: Set Up the Lagrangian. Introduce a Lagrange multiplier μ for the equality constraint $\sum_{i=1}^K q_i = 1$:

$$\mathcal{L}(\mathbf{q}, \mu) = \sum_{i=1}^K \eta_i [-(1 - q_i)^\gamma \log q_i] + \lambda \sum_{i=1}^K (q_i - \eta_i)^2 + \mu \left(\sum_{i=1}^K q_i - 1 \right). \quad (50)$$

Step 5: Compute the Partial Derivatives. For each i , compute the partial derivative of $\mathcal{L}(\mathbf{q}, \mu)$ with respect to q_i :

$$\frac{\partial \mathcal{L}}{\partial q_i} = \eta_i \left[\gamma(1 - q_i)^{\gamma-1} \log q_i + \frac{(1 - q_i)^\gamma}{q_i} \right] + 2\lambda(q_i - \eta_i) + \mu. \quad (51)$$

Set the derivative to zero at the minimizer \mathbf{q}^* :

$$\left. \frac{\partial \mathcal{L}}{\partial q_i} \right|_{\mathbf{q}=\mathbf{q}^*} = 0. \quad (52)$$

Thus:

$$\eta_i \left[\gamma(1 - q_i^*)^{\gamma-1} \log q_i^* + \frac{(1 - q_i^*)^\gamma}{q_i^*} \right] + 2\lambda(q_i^* - \eta_i) + \mu = 0. \quad (53)$$

Step 6: Analyze the Stationarity Condition. From Equation (53), we observe that for each i :

$$\eta_i \Phi(q_i^*) + 2\lambda(q_i^* - \eta_i) + \mu = 0, \quad (54)$$

where:

$$\Phi(q_i^*) = \gamma(1 - q_i^*)^{\gamma-1} \log q_i^* + \frac{(1 - q_i^*)^\gamma}{q_i^*}. \quad (55)$$

Since μ is the same for all i , we can write:

$$\eta_i \Phi(q_i^*) + 2\lambda(q_i^* - \eta_i) = -\mu \quad \forall i. \quad (56)$$

Therefore, for any i, j :

$$\eta_i \Phi(q_i^*) + 2\lambda(q_i^* - \eta_i) = \eta_j \Phi(q_j^*) + 2\lambda(q_j^* - \eta_j). \quad (57)$$

Step 7: Show the Strictly Order-Preserving Property. Suppose $q_i^* < q_j^*$. We need to show that $\eta_i < \eta_j$.

Assume, for contradiction, that $\eta_i \geq \eta_j$.

Case 1: $\eta_i = \eta_j$

From Equation (57), we have:

$$\eta_i \left[\Phi(q_i^*) - \Phi(q_j^*) \right] + 2\lambda(q_i^* - q_j^*) = 0. \quad (58)$$

Since $q_i^* < q_j^*$ and $\eta_i > 0$, we analyze the sign of $\Phi(q)$.

Observation:

- The function $\Phi(q)$ is decreasing in q over $q \in (0, 1)$.

- Therefore, $\Phi(q_i^*) > \Phi(q_j^*)$ since $q_i^* < q_j^*$.
- $q_i^* - q_j^* < 0$.

Thus, the left-hand side (LHS) is positive, which contradicts the equality to zero.

Case 2: $\eta_i > \eta_j$

Similarly, from Equation (57):

$$\left[\eta_i \Phi(q_i^*) - \eta_j \Phi(q_j^*) \right] + 2\lambda (q_i^* - \eta_i - q_j^* + \eta_j) = 0. \quad (59)$$

Since $q_i^* < q_j^*$ and $\eta_i > \eta_j$, we have:

- $q_i^* - \eta_i < q_j^* - \eta_j$ because $q_i^* < q_j^*$ and $\eta_i > \eta_j$.
- $\eta_i \Phi(q_i^*) > \eta_j \Phi(q_j^*)$ since $\eta_i > \eta_j$ and $\Phi(q_i^*) > \Phi(q_j^*)$.

Thus, the LHS is positive, leading to a contradiction.

Step 8: Conclusion. Our assumption that $\eta_i \geq \eta_j$ must be false. Therefore, if $q_i^* < q_j^*$, it must be that $\eta_i < \eta_j$.

Hence, the Focal Calibration Loss satisfies the Strictly Order-Preserving Property, and thus it is classification-calibrated. \square

A.6 Properties of $\sigma^{Y,\lambda}$

LEMMA 16. Let $\sigma^{Y,\lambda}(q)$ be defined as:

$$\sigma^{Y,\lambda}(q) = (1-q)^Y - \gamma q \log q (1-q)^{Y-1} - 2\lambda q, \quad (60)$$

where $q \in (0, 1)$, $\gamma \geq 0$, and $\lambda \geq 0$. Then, $\sigma^{Y,\lambda}(q)$ has the following properties:

- (1) $\sigma^{Y,\lambda}(q)$ is continuous and differentiable on $q \in (0, 1)$.
- (2) As $q \rightarrow 0^+$, $\sigma^{Y,\lambda}(q) \rightarrow 1$.
- (3) As $q \rightarrow 1^-$, $\sigma^{Y,\lambda}(q) \rightarrow -2\lambda$.
- (4) $\sigma^{Y,\lambda}(q)$ is strictly decreasing on $q \in (0, 1)$.
- (5) There exists a unique $q^* \in (0, 1)$ such that $\sigma^{Y,\lambda}(q^*) = 0$.

PROOF. **1. Continuity and Differentiability.**

Each term in (60) is continuous and differentiable on $q \in (0, 1)$:

- $(1-q)^Y$ is continuous and differentiable for $q \in (0, 1)$ and $\gamma \geq 0$.
- $-\gamma q \log q (1-q)^{Y-1}$ is continuous and differentiable since $\log q$ is continuous on $q \in (0, 1)$.
- $-2\lambda q$ is a linear function and thus continuous and differentiable.

Therefore, $\sigma^{Y,\lambda}(q)$ is continuous and differentiable on $q \in (0, 1)$.

2. Limit as $q \rightarrow 0^+$.

As $q \rightarrow 0^+$, we have $(1-q)^Y \rightarrow 1$, $q \log q \rightarrow 0$, and $-2\lambda q \rightarrow 0$.

$$\sigma^{Y,\lambda}(q) \rightarrow 1 - 0 + 0 = 1. \quad (61)$$

3. Limit as $q \rightarrow 1^-$.

As $q \rightarrow 1^-$, $(1-q)^Y \rightarrow 0$, $-\gamma q \log q (1-q)^{Y-1} \rightarrow 0$, and $-2\lambda q \rightarrow -2\lambda$. Therefore:

$$\sigma^{Y,\lambda}(q) \rightarrow 0 + 0 - 2\lambda = -2\lambda. \quad (62)$$

4. Strict Monotonic Decrease.

Compute the first derivative $\sigma^{Y,\lambda}(q)$:

$$\begin{aligned} \sigma^{Y,\lambda}(q) &= \frac{d}{dq} \left[(1-q)^Y - \gamma q \log q (1-q)^{Y-1} - 2\lambda q \right] \\ &= -\gamma(1-q)^{Y-1} - \gamma \log q (1-q)^{Y-1} + \gamma q \frac{1}{q} (1-q)^{Y-1} \\ &\quad + \gamma(\gamma-1)q \log q (1-q)^{Y-2} - 2\lambda \\ &= -\gamma(1-q)^{Y-1} - \gamma \log q (1-q)^{Y-1} + \gamma(1-q)^{Y-1} \\ &\quad + \gamma(\gamma-1)q \log q (1-q)^{Y-2} - 2\lambda \\ &= \gamma \left[-(1-q)^{Y-1} + (1-q)^{Y-1} \right] - \gamma \log q (1-q)^{Y-1} \\ &\quad + \gamma(\gamma-1)q \log q (1-q)^{Y-2} - 2\lambda \\ &= -\gamma \log q (1-q)^{Y-1} + \gamma(\gamma-1)q \log q (1-q)^{Y-2} - 2\lambda. \end{aligned} \quad (63)$$

Since $\log q < 0$ for $q \in (0, 1)$ and $(1-q)^{Y-1} > 0$, the first term is positive. The second term is negative or zero depending on γ :

- If $\gamma \geq 1$, then $(\gamma-1) \geq 0$, and since $\log q < 0$, the second term is negative.
- If $0 \leq \gamma < 1$, then $(\gamma-1) < 0$, but $\log q < 0$, so the product is positive; however, $q(1-q)^{Y-2}$ remains finite and positive.

Overall, $\sigma^{Y,\lambda}(q) < 0$ for all $q \in (0, 1)$, implying that $\sigma^{Y,\lambda}(q)$ is strictly decreasing on $q \in (0, 1)$.

5. Existence of a Unique Root.

Since $\sigma^{Y,\lambda}(q)$ is continuous on $[0, 1]$ and strictly decreasing from $\sigma^{Y,\lambda}(0^+) = 1$ to $\sigma^{Y,\lambda}(1^-) = -2\lambda$, by the Intermediate Value Theorem, there exists a unique $q^* \in (0, 1)$ such that $\sigma^{Y,\lambda}(q^*) = 0$. \blacksquare

COROLLARY 17. The equation $\sigma^{Y,\lambda}(q) = 0$ has exactly one solution $q^* \in (0, 1)$.

Understanding the properties of $\sigma^{Y,\lambda}(q)$ is crucial in analyzing the behavior of the Focal Calibration Loss. The function's monotonic decrease ensures a unique mapping between the predicted probabilities q and the true class probabilities η , aiding in establishing the consistency and calibration of the loss function.

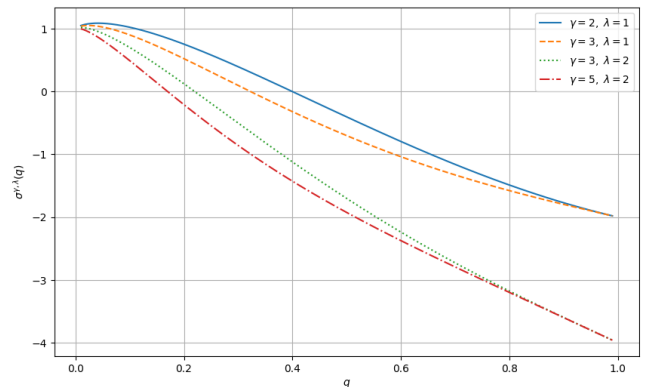


Figure 6: Plot of $\sigma^{Y,\lambda}(q)$ vs. q for different γ and λ

The analysis of $\sigma^{Y,\lambda}(q)$ confirms that the function is strictly decreasing and crosses zero exactly once in the interval $q \in (0, 1)$

in Fig. 6. This behavior is essential for ensuring that the Focal Calibration Loss provides a unique and consistent mapping between predicted probabilities and true class probabilities, contributing to the effectiveness of the loss function in classification tasks. \square

A.7 Proof of Thm. (11): The calibration loss defined as the mean squared L_2 norm is a strictly proper scoring rule for both binary and multiclass classification.

PROOF. In the proof, $Y \sim P$ denotes a random variable Y that follows the probability distribution P . The predicted probability for class k is q_k , and the true probability for class k is p_k . The expectation $\mathbb{E}_{Y \sim P}[S(Q, Y)]$ represents the expected value of the scoring function $S(Q, Y)$ over the distribution P . The calibration loss $\mathcal{L}_{\text{calib}}$ is defined as the mean squared L_2 norm, and it measures the squared differences between predicted probabilities \hat{p}_i and actual binary outcomes y_i for binary classification, or between predicted probability vectors $\hat{\mathbf{p}}_i$ and true outcome vectors \mathbf{y}_i for multiclass classification. The derivatives $\frac{\partial}{\partial q_j}$ and $\frac{\partial^2}{\partial q_j^2}$ denote the first and second partial derivatives w.r.t. the predicted probability q_j , used to find and verify the maxima of the expected score.

The L_2 norm and the Brier score are closely related. For binary classification, the squared L_2 norm of the difference between predicted probabilities \hat{p}_i and actual binary outcomes y_i is equivalent to the Brier score:

$$\frac{1}{N} \sum_{i=1}^N (\hat{p}_i - y_i)^2 \quad (64)$$

For multiclass classification, the mean squared L_2 norm is:

$$\frac{1}{N} \sum_{i=1}^N \sum_{k=1}^K (\hat{p}_{ik} - y_{ik})^2 \quad (65)$$

This is the Brier score for multiclass classification.

1) Binary Classification:

$$\mathbb{E}_{Y \sim P}[S(Q, Y)] = -P(Y = 1)(q - 1)^2 + P(Y = 0)q^2 \quad (66)$$

Let p be the true probability of the event $Y = 1$. Then, the expected score is:

$$\mathbb{E}_{Y \sim P}[S(Q, Y)] = -p(q - 1)^2 - (1 - p)q^2 \quad (67)$$

To find the maxima, take the derivative w.r.t. q and set it to zero:

$$\begin{aligned} \frac{\partial}{\partial q} \mathbb{E}_{Y \sim P}[S(Q, Y)] &= -2p(q - 1) - 2(1 - p)q \\ &= -2pq + 2p - 2q + 2pq \\ &= 2p - 2q \Rightarrow 0 = 2p - 2q \Rightarrow p = q \end{aligned} \quad (68)$$

We need to check the second derivative to see if it is a maximum (for the properness condition) and if it is the only maximizer (for the strictness condition):

$$\frac{\partial^2}{\partial q^2} \mathbb{E}_{Y \sim P}[S(Q, Y)] = -2 < 0 \quad (69)$$

The second derivative is always negative which means that the function is concave and the maximum is unique. Therefore, $p = q$ is the only maximizer and the Brier scoring rule for binary classification is strictly proper.

2) Multiclass Classification:

$$\begin{aligned} \mathbb{E}_{Y \sim P}[S(Q, Y)] &= \sum_k P(Y = k) \left[-\sum_i (q_i - y_i)^2 \right] \\ &= \sum_k P(Y = k) \left[-(q_k - 1)^2 - \sum_{i \neq k} q_i^2 \right] \\ &= \sum_k P(Y = k) \left[-(q_k - 1)^2 + q_k^2 - \sum_i q_i^2 \right] \\ &= \sum_k P(Y = k) \left[-q_k^2 - 1 + 2q_k + q_k^2 - \sum_i q_i^2 \right] \\ &= \sum_k P(Y = k) \left[2q_k - 1 - \sum_i q_i^2 \right] \\ &= \sum_k P(Y = k)(2q_k - 1) - \sum_i q_i^2 \end{aligned} \quad (70)$$

This expression can be expressed as follows by replacing q_{iK} with $1 - \sum_{i \neq K} q_i$:

$$\mathbb{E}_{Y \sim P}[S(Q, Y)] = p_1(2q_1 - 1) - q_1^2 + p_2(2q_2 - 1) - q_2^2 + \dots + p_K(2q_K - 1) - q_K^2 \quad (71)$$

Taking the derivative w.r.t. q_j and setting it to zero, we obtain:

$$\begin{aligned} \frac{\partial}{\partial q_j} \mathbb{E}_{Y \sim P}[S(Q, Y)] &= 2p_j - 2q_j - 2p_K + 2 \left(1 - \sum_{i \neq K} q_i \right) \\ &= 2p_j - 2q_j - 2p_K + 2q_K \\ &= (p_j - q_j) + (q_K - p_K) = 0 \\ &(p_j - q_j) = (p_K - q_K) \end{aligned} \quad (72)$$

We know that $\sum_i p_i = 1$ and $\sum_i q_i = 1$, therefore:

$$\begin{aligned} p_1 - q_1 = p_2 - q_2 = \dots = p_K - q_K = \lambda \\ \sum_i (p_i - q_i) = K \cdot \lambda = 0 \\ \Rightarrow \lambda = 0 \quad \text{since } K \neq 0 \\ \Rightarrow p_i = q_i \quad \text{for all } i = 1, \dots, K \end{aligned} \quad (73)$$

Now, we need to check the second derivative to see if it is a maximum (for the properness condition) and if it is the only maximizer for the strictness condition:

$$\frac{\partial^2}{\partial q_j^2} \mathbb{E}_{Y \sim P}[S(Q, Y)] = -2 - 2 = -4 < 0 \quad (74)$$

The second derivative is always negative which means that the function is concave and the maximum is unique. Therefore, $p = q$ is the only maximizer and the Brier scoring rule for multiclass classification is strictly proper. \square

A.8 Proof that the Focal Calibration Loss is Strictly Proper

PROOF. We aim to show that $\mathcal{L}_{\text{FCL}}^{Y,\lambda}$ is minimized if and only if $\hat{\mathbf{p}} = \mathbf{y}$ when $\lambda > 0$ and $\gamma > 0$, and that it is not strictly proper when $\lambda = 0$.

Case 1: $\lambda > 0$. Let $\mathbf{y} \in \Delta^K$ be the true probability vector, and $\hat{\mathbf{p}} \in \Delta^K$ be the predicted probability vector. We consider two scenarios: (a) When $\hat{\mathbf{p}} = \mathbf{y}$. At $\hat{\mathbf{p}} = \mathbf{y}$, the calibration loss is:

$$\mathcal{L}_{\text{calib}}(\mathbf{y}, \mathbf{y}) = \|\mathbf{y} - \mathbf{y}\|_2^2 = 0. \quad (75)$$

Assuming \mathbf{y} is a one-hot vector with $y_j = 1$ for the true class j , the focal loss becomes:

$$\mathcal{L}_{\text{focal}}^Y(\mathbf{y}, \mathbf{y}) = -(1 - y_j)^Y \log y_j = -0^Y \cdot 0 = 0. \quad (76)$$

Thus, the total loss is:

$$\mathcal{L}_{\text{FCL}}^{Y,\lambda}(\mathbf{y}, \mathbf{y}) = 0 + \lambda \cdot 0 = 0. \quad (77)$$

(b) When $\hat{\mathbf{p}} \neq \mathbf{y}$. The calibration loss is strictly positive:

$$\mathcal{L}_{\text{calib}}(\hat{\mathbf{p}}, \mathbf{y}) = \|\hat{\mathbf{p}} - \mathbf{y}\|_2^2 > 0. \quad (78)$$

The focal loss for the true class j satisfies:

$$\mathcal{L}_{\text{focal}}^Y(\hat{\mathbf{p}}, \mathbf{y}) = -(1 - \hat{p}_j)^Y \log \hat{p}_j > 0 \quad \text{for } \hat{p}_j < 1. \quad (79)$$

Thus, the total loss is:

$$\mathcal{L}_{\text{FCL}}^{Y,\lambda}(\hat{\mathbf{p}}, \mathbf{y}) = \mathcal{L}_{\text{focal}}^Y(\hat{\mathbf{p}}, \mathbf{y}) + \lambda \mathcal{L}_{\text{calib}}(\hat{\mathbf{p}}, \mathbf{y}) > 0. \quad (80)$$

Conclusion for $\lambda > 0$: Since the loss $\mathcal{L}_{\text{FCL}}^{Y,\lambda}$ attains its unique global minimum of zero when $\hat{\mathbf{p}} = \mathbf{y}$, it is strictly proper when $\lambda > 0$.

Case 2: $\lambda = 0$. When $\lambda = 0$, the FCL reduces to the focal loss:

$$\mathcal{L}_{\text{FCL}}^{Y,0}(\hat{\mathbf{p}}, \mathbf{y}) = \mathcal{L}_{\text{focal}}^Y(\hat{\mathbf{p}}, \mathbf{y}). \quad (81)$$

The focal loss is not strictly proper because:

(a) Multiple Minimizers: Consider any $\hat{\mathbf{p}}$ where $\hat{p}_j = 1$ and $\hat{p}_k = 0$ for $k \neq j$. In this case:

$$\mathcal{L}_{\text{focal}}^Y(\hat{\mathbf{p}}, \mathbf{y}) = 0. \quad (82)$$

However, suppose $\hat{p}_j = q < 1$ but still significantly higher than other \hat{p}_k . Depending on γ , the focal loss may not penalize this deviation strongly, and $\mathcal{L}_{\text{focal}}^Y(\hat{\mathbf{p}}, \mathbf{y})$ may still be close to zero. Therefore, the minimum loss may not be uniquely attained at $\hat{\mathbf{p}} = \mathbf{y}$.

(b) Lack of Strict Convexity: The focal loss is not strictly convex with respect to $\hat{\mathbf{p}}$, especially when $\gamma = 0$, where it reduces to the cross-entropy loss, which is proper but not strictly proper without additional regularization.

Conclusion for $\lambda = 0$: Since the minimum of $\mathcal{L}_{\text{FCL}}^{Y,0}$ is not uniquely achieved at $\hat{\mathbf{p}} = \mathbf{y}$, the loss is not strictly proper when $\lambda = 0$.

Overall Conclusion. The Focal Calibration Loss $\mathcal{L}_{\text{FCL}}^{Y,\lambda}$ is strictly proper if and only if $\lambda > 0$ and $\gamma > 0$. \square

A.9 Focal Loss Relative with Entropy Regularised KL Divergence

This section we illustrate why focal loss tends to favor accurate yet less confident solutions. We demonstrate that it inherently balances minimizing the KL-divergence and maximizing the entropy based on the parameter γ . Let \mathcal{L}_f represent the focal loss with parameter γ , and \mathcal{L}_c represent the cross-entropy loss between $\hat{\mathbf{p}}$ and q . Here, K denotes the number of classes, and q_k and \hat{p}_k represent the ground-truth and predicted probabilities for the k -th class, respectively. We consider the following straightforward extension of focal loss:

$$\begin{aligned} \mathcal{L}_{\text{focal}}(\hat{\mathbf{p}}, \mathbf{y}) &= - \sum_{k=1}^K y_{ik} (1 - \hat{p}_{ik})^Y \log \hat{p}_{ik} \\ &\geq - \sum_{k=1}^K y_{ik} (1 - \gamma \hat{p}_{ik}) \log \hat{p}_{ik} \end{aligned}$$

By Bernoulli's inequality $\forall \gamma \geq 1$, since $\hat{p}_{ik} \in [0, 1]$

$$\begin{aligned} &= - \sum_{k=1}^K y_{ik} \log \hat{p}_{ik} - \gamma \left| \sum_{k=1}^K y_{ik} \hat{p}_{ik} \log \hat{p}_{ik} \right| \quad \forall k, \log \hat{p}_{ik} \leq 0 \\ &\geq - \sum_{k=1}^K y_{ik} \log \hat{p}_{ik} + \gamma \sum_{k=1}^K \hat{p}_{ik} \log \hat{p}_{ik} = \mathcal{L}_c - \gamma H[\hat{\mathbf{p}}] \end{aligned}$$

By Hölder's inequality $\|fg\|_1 \leq \|f\|_\infty \|g\|_1$

(83)

Given that $\mathcal{L}_c = KL(q\|\hat{\mathbf{p}}) + H[q]$, combining it to inequality Eq. (83):

$$\mathcal{L}_{\text{focal}}(\hat{\mathbf{p}}, \mathbf{y}) \geq KL(q\|\hat{\mathbf{p}}) + H[q] - \gamma H[\hat{\mathbf{p}}] \quad (84)$$

In the case of one-hot encoding (Delta distribution for q), focal loss will maximize $-\hat{p}_k \log \hat{p}_k$ (let k be the ground-truth class index), the component of the entropy of $\hat{\mathbf{p}}$ corresponding to the ground-truth index. Thus, it will prefer learning $\hat{\mathbf{p}}$ such that \hat{p}_k is assigned a higher value (because of the KL term), but not too high (because of the entropy term), and will ultimately avoid preferring overconfident models (by contrast to cross-entropy loss).

A.10 Hyperparameter Selection for Focal Calibration Loss

Table 5: γ and λ Selection

Dataset	Model	γ	λ
CIFAR-100	ResNet-50	2.0	0.5
	ResNet-110	4.0	1.5
	Wide-ResNet-26-10	3.0	0.5
	DenseNet-121	3.0	0.5
CIFAR-10	ResNet-50	4.0	1.5
	ResNet-110	4.0	1.5
	Wide-ResNet-26-10	2.0	0.5
	DenseNet-121	2.0	0.5
Tiny-ImageNet	ResNet-50	3.0	0.5
20 Newsgroups	Global Pooling CNN	5.0	4.5
AG News	Global Pooling CNN	4.0	3.0
FinSen	Global Pooling CNN	4.0	4.0

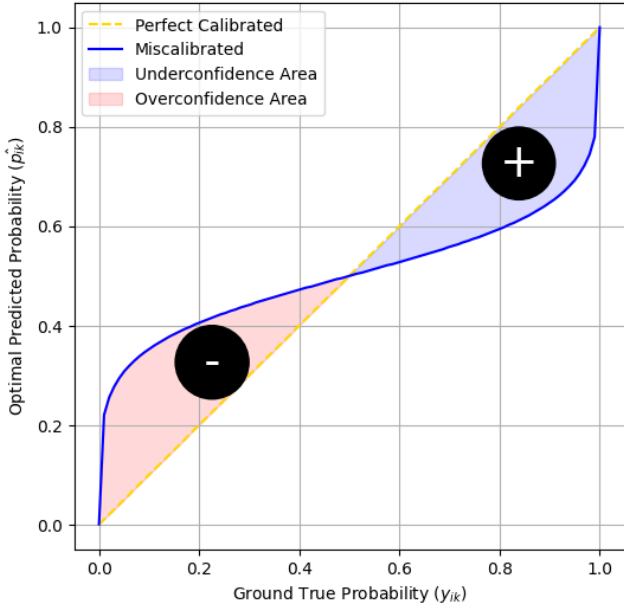


Figure 7: Optimal Predicted Probability (\hat{p}_{ik}) for Various Values of Ground True Probability (y_{ik}) with Calibration Analysis. Circular markers with "+" and "-" signs represent the areas where the calibration term increases or decreases in visualizing how it adjust the predicted probabilities.

A.11 Decision Boundary on Focal Loss and Focal Calibration Loss (FCL)

We compared the decision boundaries of a neural network trained with Focal Loss (FL) and Focal Calibration Loss (FCL) on a noisy, hard-to-classify synthetic dataset, using the same $\gamma = 10$ for both models. The dataset, generated with noise=0.2, created overlapping classes that are difficult to separate. Both models were trained using a simple feedforward neural network with two hidden layers of 10 units and optimized with Adam for 500 epochs. While the FL model generated sharp decision boundaries focusing on hard samples, the FCL model, with $\lambda = 1.5$, produced a smoother boundary as depicted in Fig. 8, effectively balancing accuracy and calibration.

A.12 Table 6 AdaECE Evaluation Result

A.13 Table 7 Classwise-ECE Evaluation Result

A.14 Proof of Thm. (13): Post-Processing Gap of focal calibration loss and focal loss

PROOF. Let the post-processed prediction be defined as $\kappa(\hat{p}_{ik}) = \hat{p}_{ik} + \eta(\hat{p}_{ik})$, where $\eta(\hat{p}_{ik})$ is the post-processing adjustment function applied to the predicted probability \hat{p}_{ik} . This gives the post-processed version of the focal calibration loss (FCL) as:

$$\mathcal{L}_{\text{FCL}}^{\gamma, \lambda}(\kappa(\hat{\mathbf{p}}), \mathbf{y}) = \mathcal{L}_{\text{focal}}(\kappa(\hat{\mathbf{p}}), \mathbf{y}) + \lambda \mathcal{L}_{\text{calib}}(\kappa(\hat{\mathbf{p}}), \mathbf{y}) \quad (85)$$

where $\mathcal{L}_{\text{focal}}$ is the focal loss, $\mathcal{L}_{\text{calib}}$ is the calibration loss, and $\lambda \geq 0$ is a weighting parameter controlling the calibration term.

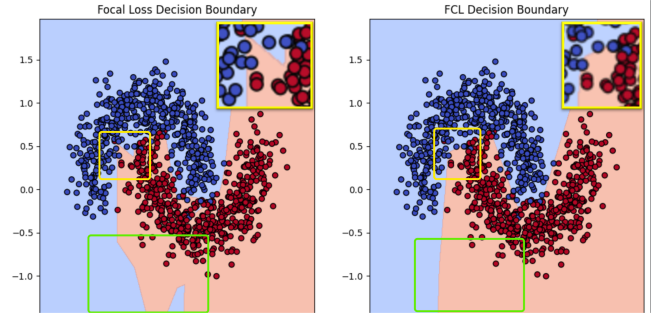


Figure 8: Decision boundary comparison between Focal Loss (left) and Focal Calibration Loss (FCL) (right) on a synthetic dataset with hard samples. In both models, blue and red regions represent the areas classified as Class 0 and Class 1, respectively. The yellow boxes highlight regions where hard samples from both classes overlap, and the green boxes indicate areas where FCL provides a smoother decision boundary compared to Focal Loss.

Following Definition 5, the post-processing gap for the FCL $\text{pGap}_{\mathcal{D}}(\mathcal{L}_{\text{FCL}}^{\gamma, \lambda})$ is defined as:

$$\mathbb{E}_{(x, y) \sim \mathcal{D}}[\mathcal{L}_{\text{FCL}}^{\gamma, \lambda}(f(x), y)] - \mathbb{E}_{(x, y) \sim \mathcal{D}}[\mathcal{L}_{\text{FCL}}^{\gamma, \lambda}(\kappa(f(x)), y)] \quad (86)$$

Step 1: Expanding the Post-Processing Gap for FCL. Substituting the definition of the focal calibration loss, we obtain:

$$\begin{aligned} \text{pGap}_{\mathcal{D}}(\mathcal{L}_{\text{FCL}}^{\gamma, \lambda}) &= \mathbb{E}_{(x, y) \sim \mathcal{D}}[\mathcal{L}_{\text{focal}}(f(x), y)] \\ &\quad + \lambda \mathbb{E}_{(x, y) \sim \mathcal{D}}[\mathcal{L}_{\text{calib}}(f(x), y)] \\ &\quad - \mathbb{E}_{(x, y) \sim \mathcal{D}}[\mathcal{L}_{\text{focal}}(\kappa(f(x)), y)] \\ &\quad - \lambda \mathbb{E}_{(x, y) \sim \mathcal{D}}[\mathcal{L}_{\text{calib}}(\kappa(f(x)), y)] \end{aligned} \quad (87)$$

Step 2: Special Case when $\lambda = 0$. When $\lambda = 0$, the focal calibration loss simplifies to the focal loss, as the calibration term is removed. Thus, the post-processing gap for FCL reduces to the post-processing gap for FL:

$$\text{pGap}_{\mathcal{D}}(\mathcal{L}_{\text{FCL}}^{\gamma, \lambda=0}) = \text{pGap}_{\mathcal{D}}(\mathcal{L}_{\text{focal}}) \quad (88)$$

Step 3: General Case when $\lambda > 0$. When $\lambda > 0$, the calibration term influences the post-processing gap by helping to reduce the calibration error. We focus on the term:

$$\lambda \left(\mathbb{E}_{(x, y) \sim \mathcal{D}}[\mathcal{L}_{\text{calib}}(f(x), y)] - \mathbb{E}_{(x, y) \sim \mathcal{D}}[\mathcal{L}_{\text{calib}}(\kappa(f(x)), y)] \right) \quad (89)$$

This term measures the improvement in calibration achieved through post-processing κ . The calibration loss, $\mathcal{L}_{\text{calib}}(f(x), y)$, can be defined as a squared loss: $\mathcal{L}_{\text{calib}}(\hat{\mathbf{p}}, \mathbf{y}) = \sum_{k=1}^K (y_{ik} - \hat{p}_{ik})^2$.

Thus, the calibration gap $\text{pGap}_{\mathcal{D}}(\mathcal{L}_{\text{calib}})$ becomes:

$$\begin{aligned} &\mathbb{E}_{(x, y) \sim \mathcal{D}} \left[\sum_{k=1}^K (y_{ik} - \hat{p}_{ik})^2 \right] - \mathbb{E}_{(x, y) \sim \mathcal{D}} \left[\sum_{k=1}^K (y_{ik} - \kappa(\hat{p}_{ik}))^2 \right] \\ &= \mathbb{E}_{(x, y) \sim \mathcal{D}} \left[\sum_{k=1}^K (y_{ik} - \hat{p}_{ik})^2 - (y_{ik} - \hat{p}_{ik} - \eta(\hat{p}_{ik}))^2 \right] \end{aligned} \quad (90)$$

Table 6: ↓ AdaECE (%) for various methods both before (pre) and after (post) applying temperature scaling.

Dataset	Model	Weight Decay[12]		Brier Loss[5]		MMCE[22]		Label Smooth[43]		Focal Loss - 53[32]		Dual Focal[44]		Focal Calibration	
		Pre T	Post T	Pre T	Post T	Pre T	Post T	Pre T	Post T	Pre T	Post T	Pre T	Post T	Pre T	Post T
CIFAR-100	ResNet-50	17.99	3.38(2.2)	5.46	4.24(1.1)	15.05	3.42(1.9)	6.72	5.37(1.1)	5.64	2.84(1.1)	8.79	2.27(1.3)	3.74	2.11(1.1)
	ResNet-110	19.28	6.27(2.3)	6.51	3.75(1.2)	18.83	4.86(2.3)	9.68	8.11(1.3)	10.90	4.13(1.3)	11.64	4.48(1.3)	4.88	3.27(1.1)
	Wide-ResNet-26-10	15.16	3.23(2.1)	4.08	3.11(1.1)	13.55	3.83(2.0)	3.73	3.73(1.0)	2.40	2.38(1.1)	5.36	2.38(1.2)	2.35	2.35(1.0)
	DenseNet-121	19.07	3.82(2.2)	3.92	2.41(1.1)	17.37	3.07(2.0)	8.62	5.92(1.1)	3.35	1.80(1.1)	6.69	1.69(1.2)	1.47	1.47(1.0)
CIFAR-10	ResNet-50	4.22	2.11(2.5)	1.85	1.34(1.1)	4.67	2.01(2.6)	4.28	3.20(0.9)	1.64	1.64(1.0)	1.28	1.28(1.0)	0.75	0.75(1.0)
	ResNet-110	4.78	2.42(2.6)	2.52	1.72(1.2)	5.21	2.66(2.8)	4.57	3.62(0.9)	1.76	1.32(1.1)	1.69	1.42(1.1)	1.25	1.25(1.0)
	Wide-ResNet-26-10	3.22	1.62(2.2)	1.94	1.94(1.0)	3.58	1.83(2.2)	4.58	2.55(0.8)	1.84	1.63(0.9)	3.16	1.20(0.8)	1.39	1.39(1.0)
	DenseNet-121	4.69	2.28(2.4)	1.84	1.84(1.0)	4.97	2.69(2.4)	4.60	3.36(0.9)	1.58	1.62(0.9)	0.79	1.32(0.9)	1.28	1.28(1.0)
Tiny-ImageNet	ResNet-50	16.02	4.99(1.5)	5.00	3.60(0.9)	13.15	4.73(1.3)	15.05	5.36(0.7)	1.31	1.31(1.0)	2.66	2.66(1.0)	10.22	1.34(0.8)
NLP 20 Newsgroups	Global Pooling CNN	17.91	2.23(3.4)	13.57	3.11(2.3)	15.21	6.47(2.2)	4.39	2.63(1.1)	8.65	3.78(1.5)	18.44	3.81(2.3)	15.29	1.48(2.2)
NLP AG News	Global Pooling CNN	4.77	0.67(2.0)	6.78	2.77(2.8)	1.80	1.78(1.1)	3.84	1.70(0.8)	6.69	0.57(3.0)	2.99	2.51(0.8)	0.97	0.38(1.1)
NLP FinSen	Global Pooling CNN	0.91	0.24(2.5)	0.35	0.35(1.0)	1.23	0.37(0.5)	4.39	4.5(0.6)	0.28	0.43(0.9)	0.23	0.43(0.7)	0.46	0.24(1.3)

Table 7: ↓ Classwise-ECE (%) for various methods both before (pre) and after (post) applying temperature scaling.

Dataset	Model	Weight Decay[12]		Brier Loss[5]		MMCE[22]		Label Smooth[43]		Focal Loss - 53[32]		Dual Focal[44]		Focal Calibration	
		Pre T	Post T	Pre T	Post T	Pre T	Post T	Pre T	Post T	Pre T	Post T	Pre T	Post T	Pre T	Post T
CIFAR-100	ResNet-50	0.39	0.22(2.2)	0.21	0.22(1.1)	0.34	0.22(1.9)	0.21	0.22(1.1)	0.21	0.20(1.1)	0.24	0.22(1.3)	0.19	0.19(1.1)
	ResNet-110	0.42	0.21(2.3)	0.22	0.23(1.2)	0.41	0.22(2.3)	0.25	0.23(1.3)	0.27	0.22(1.3)	0.28	0.21(1.3)	0.20	0.21(1.1)
	Wide-ResNet-26-10	0.34	0.21(2.1)	0.19	0.20(1.1)	0.31	0.21(2.0)	0.20	0.20(1.0)	0.18	0.20(1.1)	0.19	0.20(1.2)	0.20	0.20(1.0)
	DenseNet-121	0.42	0.22(2.2)	0.21	0.21(1.1)	0.39	0.23(2.0)	0.23	0.21(1.1)	0.20	0.21(1.1)	0.22	0.21(1.2)	0.19	0.19(1.0)
CIFAR-10	ResNet-50	0.87	0.37(2.5)	0.46	0.39(1.1)	0.97	0.55(2.6)	0.80	0.54(0.9)	0.41	0.41(1.0)	0.45	0.45(1.0)	0.36	0.36(1.0)
	ResNet-110	1.00	0.54(2.6)	0.55	0.46(1.2)	1.08	0.60(2.8)	0.75	0.50(0.9)	0.48	0.46(1.1)	0.46	0.52(1.1)	0.38	0.38(1.0)
	Wide-ResNet-26-10	0.68	0.34(2.2)	0.37	0.37(1.0)	0.77	0.41(2.2)	0.95	0.37(0.8)	0.44	0.34(0.9)	0.82	0.33(0.8)	0.33	0.33(1.0)
	DenseNet-121	0.98	0.54(2.4)	0.43	0.43(1.0)	1.02	0.53(2.4)	0.75	0.48(0.9)	0.43	0.41(0.9)	0.40	0.41(0.9)	0.37	0.37(1.0)
Tiny-ImageNet	ResNet-50	0.23	0.17(1.5)	0.17	0.16(0.9)	0.21	0.17(1.3)	0.21	0.17(0.7)	0.16	0.16(1.0)	0.16	0.16(1.0)	0.19	0.16(0.8)
NLP 20 Newsgroups	Global Pooling CNN	1.95	0.83(3.4)	1.56	0.82(2.3)	1.77	1.10(2.2)	0.93	0.91(1.1)	1.40	1.19(1.5)	2.01	1.04(2.3)	1.71	0.80(2.2)
NLP AG News	Global Pooling CNN	2.49	0.86(2.0)	3.46	1.64(2.8)	1.07	0.96(1.1)	2.69	1.57(0.8)	3.39	0.77(3.0)	2.43	1.92(0.8)	0.86	1.02(1.1)
NLP FinSen	Global Pooling CNN	0.18	0.16(2.5)	0.17	0.17(1.0)	0.32	0.19(0.5)	0.82	0.18(0.6)	0.15	0.16(0.9)	0.17	0.16(0.7)	0.15	0.15(1.3)

Step 4: Simplifying $p\text{Gap}_{\mathcal{D}}(\mathcal{L}_{\text{calib}})$. Expanding the square term, we get:

$$\begin{aligned} & \mathbb{E}_{(x,y) \sim \mathcal{D}} \left[\sum_{k=1}^K \left((y_{ik} - \hat{p}_{ik})^2 - \left((y_{ik} - \hat{p}_{ik})^2 - 2(y_{ik} - \hat{p}_{ik})\eta(\hat{p}_{ik}) + \eta(\hat{p}_{ik})^2 \right) \right) \right] \\ &= \mathbb{E}_{(x,y) \sim \mathcal{D}} \left[\sum_{k=1}^K 2(y_{ik} - \hat{p}_{ik})\eta(\hat{p}_{ik}) - \eta(\hat{p}_{ik})^2 \right] \end{aligned} \quad (91)$$

Thus, the total post-processing gap becomes:

$$\begin{aligned} p\text{Gap}_{\mathcal{D}}(\mathcal{L}_{\text{FCL}}^{\gamma, \lambda}) &= p\text{Gap}_{\mathcal{D}}(\mathcal{L}_{\text{focal}}) + \lambda p\text{Gap}_{\mathcal{D}}(\mathcal{L}_{\text{calib}}) \\ p\text{Gap}_{\mathcal{D}}(\mathcal{L}_{\text{calib}}) &= \mathbb{E}_{(x,y) \sim \mathcal{D}} \left[\sum_{k=1}^K \underbrace{2(y_{ik} - \hat{p}_{ik})\eta(\hat{p}_{ik})}_{\text{CalibError}} - \eta(\hat{p}_{ik})^2 \right] \end{aligned} \quad (92)$$

Step 5: Analyzing Overconfidence (OC) Cases. When $\hat{p}_{ik} > y_{ik}$, $\eta(\hat{p}_{ik}) > 0$. In this case, the term $2(y_{ik} - \hat{p}_{ik})\eta(\hat{p}_{ik})$ is negative, and $-\eta(\hat{p}_{ik})^2 < 0$, which means that the calibration term overall is negative. This reduction in the post-processing gap brings the prediction closer to the true label, reducing the pGap.

Step 6: Analyzing Underconfidence (UC) Case. When $\hat{p}_{ik} < y_{ik}$, $\eta(\hat{p}_{ik}) > 0$, and thus $2(y_{ik} - \hat{p}_{ik})\eta(\hat{p}_{ik})$ is positive. This positive term increases the predicted value, reducing the gap between \hat{p}_{ik}

and y_{ik} . Additionally, the term $-\eta(\hat{p}_{ik})^2$ is still negative but smaller in magnitude, ensuring that the gap is reduced.

Since $\mathbb{E}_{(x,y) \sim \mathcal{D}} \left[\sum_{k=1}^K 2(y_{ik} - \hat{p}_{ik})\eta(\hat{p}_{ik}) - \eta(\hat{p}_{ik})^2 \right]$ ensures that pGap is not increased, maintaining or reducing the gap, as depicted in Fig. 7, we conclude that:

$$p\text{Gap}_{\mathcal{D}}(\mathcal{L}_{\text{FCL}}) \leq p\text{Gap}_{\mathcal{D}}(\mathcal{L}_{\text{focal}}). \quad (93)$$

□

A.15 Reliability Diagram and ROC Diagram

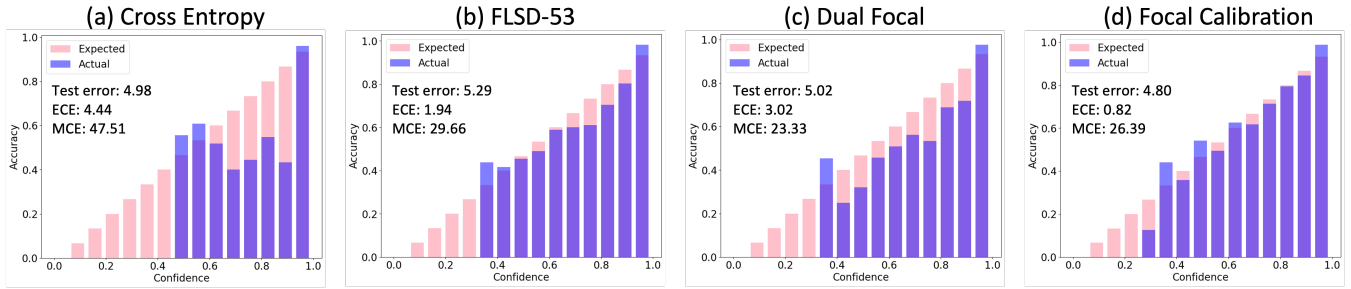


Figure 9: Reliability Diagram of Various Methods before Temperature Scaling(CIFAR10, ResNet-110, 300 Epochs).

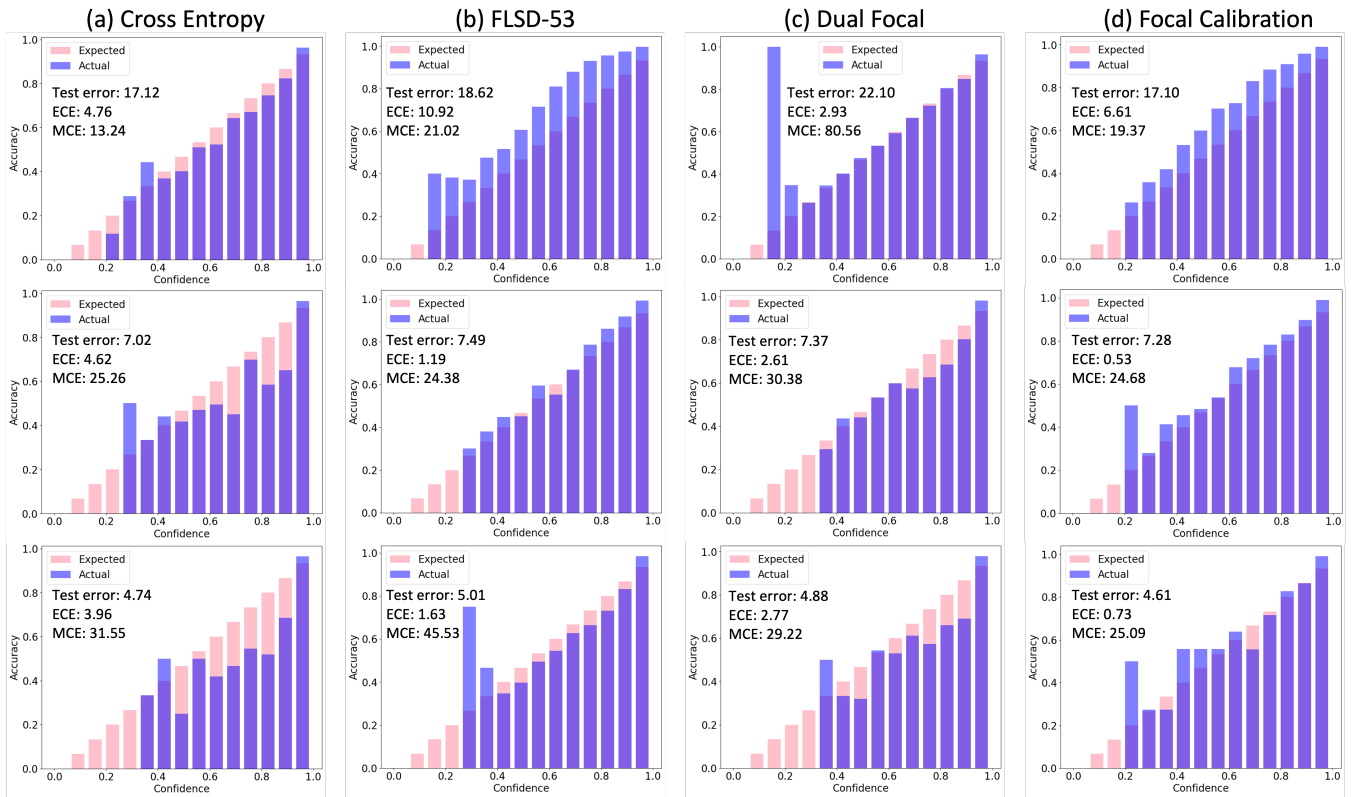


Figure 10: Reliability Diagram of Various Methods before Temperature Scaling (CIFAR10, ResNet-50, 100 - 300 Epochs). The top/middle/bottom row corresponds to the results at 100/200/300 epochs. Each row shows the performance of Cross Entropy, FLSD-53, Dual Focal Loss, and Focal Calibration Loss.

Calibrating Deep Neural Network using Euclidean Distance

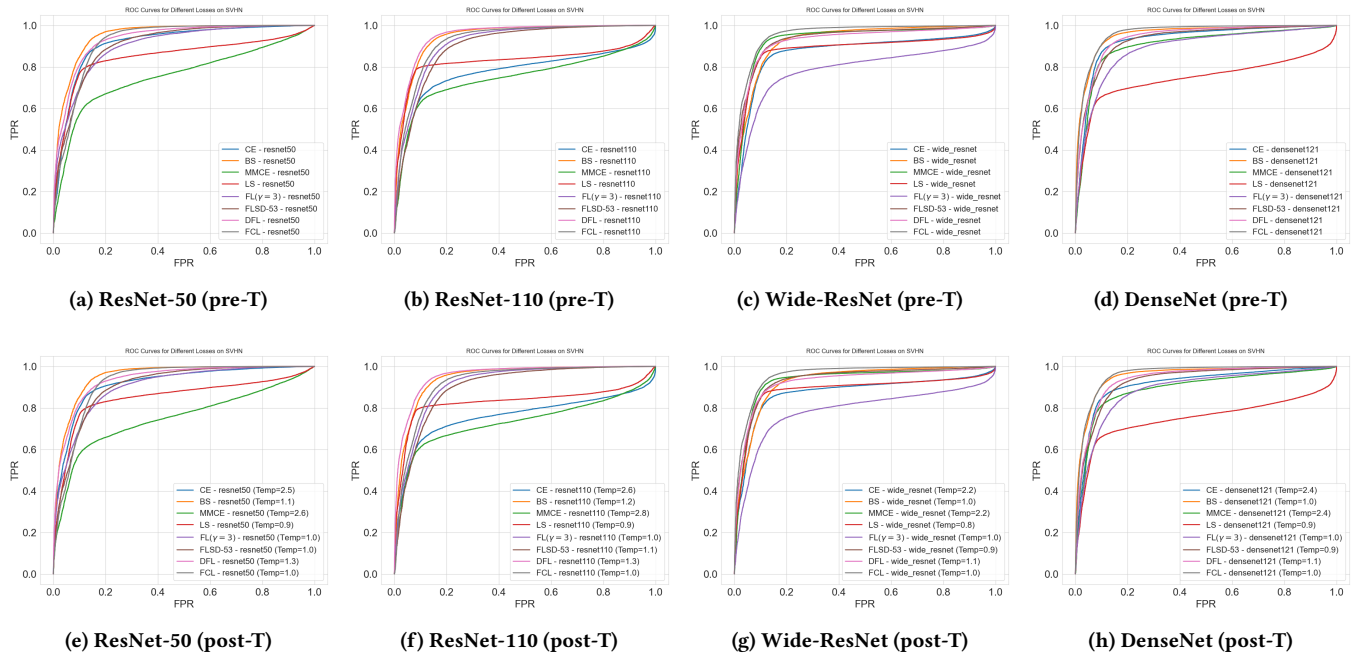


Figure 11: ROC plots obtained from Different architectures trained on CIFAR-10 and tested on SVHN

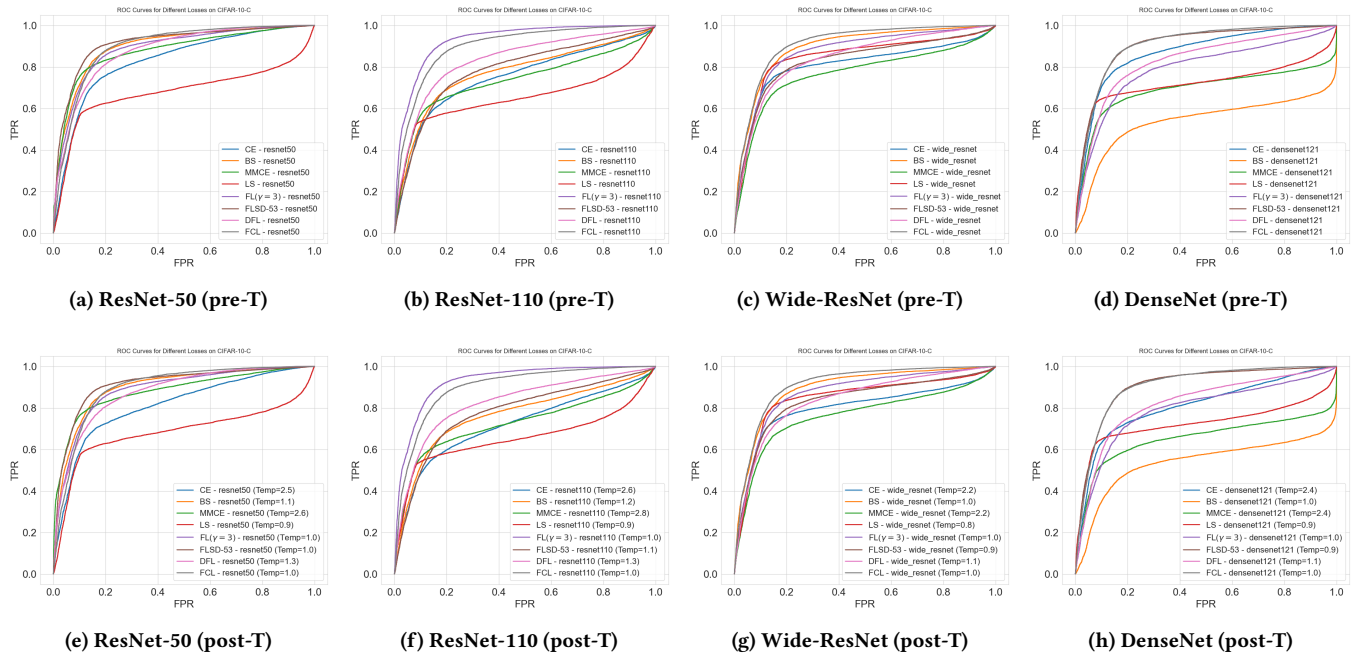


Figure 12: ROC plots obtained from Different architectures trained on CIFAR-10 and tested on CIFAR-10-C (OoD)